ACS OMEGA

http://pubs.acs.org/journal/acsodf

Article

Shift in the Mode of Carbon Cycling Recorded by Biomarkers and Carbon Isotopic Compositions in the Yanchang Formation, Ordos Basin: Autotrophy vs Heterotrophy

Huiyuan Xu,* Quanyou Liu,* Zhiquan Li,* Dujie Hou,* Xu Han,* Peng Li, Pengpeng Li, and Biqing Zhu

Cite This: *ACS Omega* 2023, 8, 5820−5835

Read Online

ACCESS | Metrics & More | Article Recommendations

ABSTRACT: Organic-rich shales and mudstones have long been investigated regarding the control of source, environment, climate, etc. on the enrichment of organic carbon. However, little is documented about how autotrophy and heterotrophy influence organic carbon cycling/export. Here, we show molecular and carbon isotopic compositional changes of the shale or mudstone source rocks from the Chang 3 to 7 members of the Yanchang Formation. The Chang 7 member source rocks have higher quality (480−500 mg/g) and total organic carbon (TOC) (15.3% on average) than other member source rocks; the sterane/hopane ratio and the $\delta^{13}C$ of organic carbon and kerogen decrease from the Chang 3 to 7 members, but $\Delta\delta$ ([average $\delta^{13}C$ of n-C_{17} + n-C_{18}] − [average $\delta^{13}C$ of pristane + phytane]) increases, and no aryl isoprenoids and C_{40} aromatic carotenoids (e.g., isorenieratane) were observed. These low maturity biomarker features suggest that there were no water stratification, photic zone euxinia (PZE), and no obvious change in the organic matter source, and the water column is generally anoxic. A comparison of the $\delta^{13}C$ of Pr and Ph with the $\delta^{13}C$ of the n-C17 and n-C18 alkanes reveals a shift in the mode of carbon cycling/export (autotrophy versus heterotrophy) in the Yanchang Formation and that there was dominant heterotrophic bacterial activity or bacterial biomass in the Chang 7 member. The TOC spike in the Chang 7 member may result from boosted carbon cycling/export that improves organic carbon preservation than other members. Possible external forcings on the shift are abundant hydrothermal- or volcanic-derived metal salts as electron acceptors in the palaeowater, which is a reasonable explanation for enhanced heterotrophic bacterial activity. This finding improves our understanding of heterotrophic bacterial activity control on organic matter (OM) preservation and may be a significant supplement for understanding the ecological or environmental forcings in the Yanchang Formation, Ordos Basin.

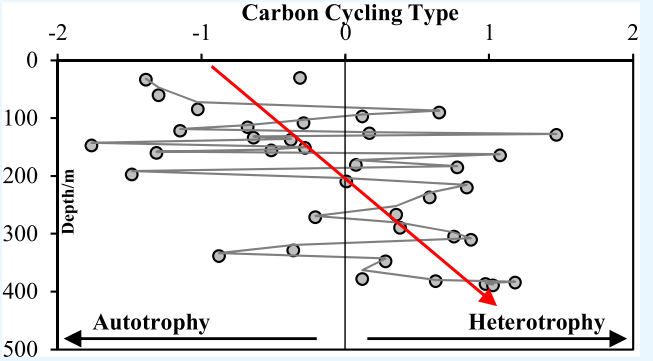

1. INTRODUCTION

Photosynthesis has been the most important form of primary production for at least the last 3.5 Gyr,[1] using light energy to convert CO_2 into organic matter. Chemosynthesis (the use of chemical rather than light energy for carbon fixation) also contributes partially, but not significantly, on a global scale.[2] Most photosynthetic organisms are aerobic: vascular plants, macro-algae (seaweeds), unicellular algae (phytoplankton), cyanobacteria, and chlorophytes. Therefore, in addition to light which is a key factor in primary production, water is essential for all life and provides hydrogen for aerobic photosynthesis. Microorganisms are the main source of organic matter, with algae, bacteria, and plankton being the most important primary producers in palaeolake and open sea. Algae have been long discussed, including the types of algal species and their corresponding environments in the water column. However, there is still a need for detailed investigation on the modification and eventual enrichment of organic matter by bacteria, especially anaerobic heterotrophic bacteria.

Canonical mechanisms of organic matter enrichment include productivity, preservation conditions, and suitable terrigenous influx.[3] Pedersen and Calvert[4] considered primary productivity as the main controlling factor for organic matter enrichment, and Tyson and Pearson[5] considered sedimentation or anoxic conditions of bottom water as the main controlling factor. The enrichment of organic matter is mainly the result of the

Received: November 23, 2022
Accepted: January 20, 2023
Published: February 2, 2023

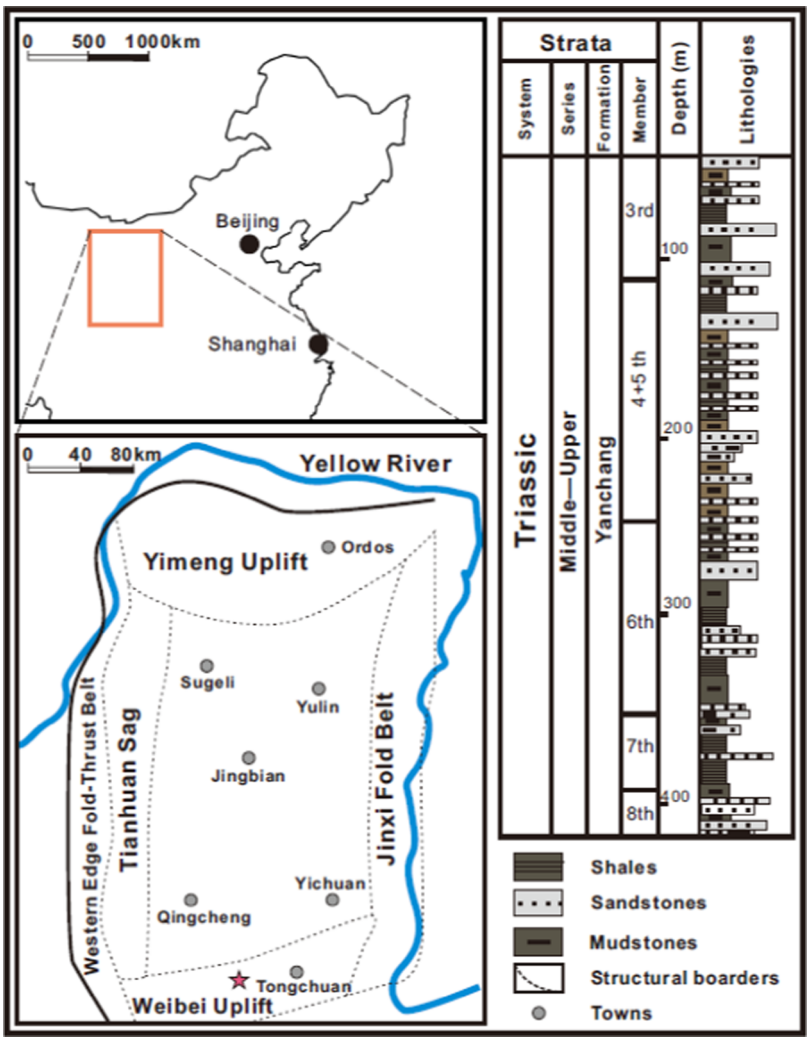

Figure 1. Location map of the Ordos Basin showing the position of the subdivided tectonic units, the Z101 well, the structural elements, and the generalized stratigraphic chart showing the Chang 3 to Chang 8 members.

combination of organic matter sources and preservation conditions, and different types of basins may have different main controlling factors. Organic matter sources are often closely related to primary productivity, nutrient elements, geological events, etc. Organic matter preservation conditions are often related to water stratification, the salinization of water bodies, redox conditions, etc.

Organic-rich deposition of the Triassic Yanchang Formation is likely to be controlled by a range of geological events (such as marine transgression, anoxia, algal bloom, volcanic eruptions, deep hydrothermal activity, etc.).[6,7] The Triassic Yanchang Formation has developed the most important hydrocarbon-rich shale in central and western China. The shale at the Chang 7 member of the Upper Triassic Yanchang Formation has high total organic carbon (TOC). It provides the main source of oil for the Mesozoic petroleum system.[8,9] In addition to the organic-rich shales, many tuff intervals were observed at the bottom of the Chang 7 member, which is indicative of frequent volcanic eruptions.[6] Several other specific lithologies are observed in the organic-rich strata, including seismic turbidites, siliciclastic rocks, and microcrystalline dolomite layers, which are associated with major geologic events such as volcanic activity. The fertilization effect during volcanic eruptions greatly stimulates microbial growth due to nutrient-rich volcanic ash.[10] This is different from the model of high primary productivity caused by the oceanic upwelling or the model of organic preservation in the stratified water column.[11]

Previous studies have focused on organic-rich source rocks of the Yanchang Formation to explore the mechanism of organic matter enrichment from the perspective of the palaeowater environment and palaeo-geological events to distinguish between the differences of organic matter enrichment in different submembers (Chang 1−7) and to clarify the control of elements on organic matter enrichment. However, molecular geochemical studies remain underappreciated in filling the gap between microbial respiration and organic matter enrichment.

Carbon reflects the source of CO_2 and its producer's fractionation pathway. Biomarkers, especially diagnostic biomarkers and their stable carbon isotopic compositions, can distinguish the fixation or reworking pathway of organic carbon. In this work, the Yanchang Formation shales will be analyzed to study the influence of ecological characteristics of microorganisms such as algae and bacteria on organic matter enrichment. This study also spells out the evolutionary processes of life and biogeochemical processes during the formation of the Yanchang shales, searching for the key relationship between the biological structure and the preservation of organic matter.

https://doi.org/10.1021/acsomega.2c07382
ACS Omega 2023, 8, 5820−5835

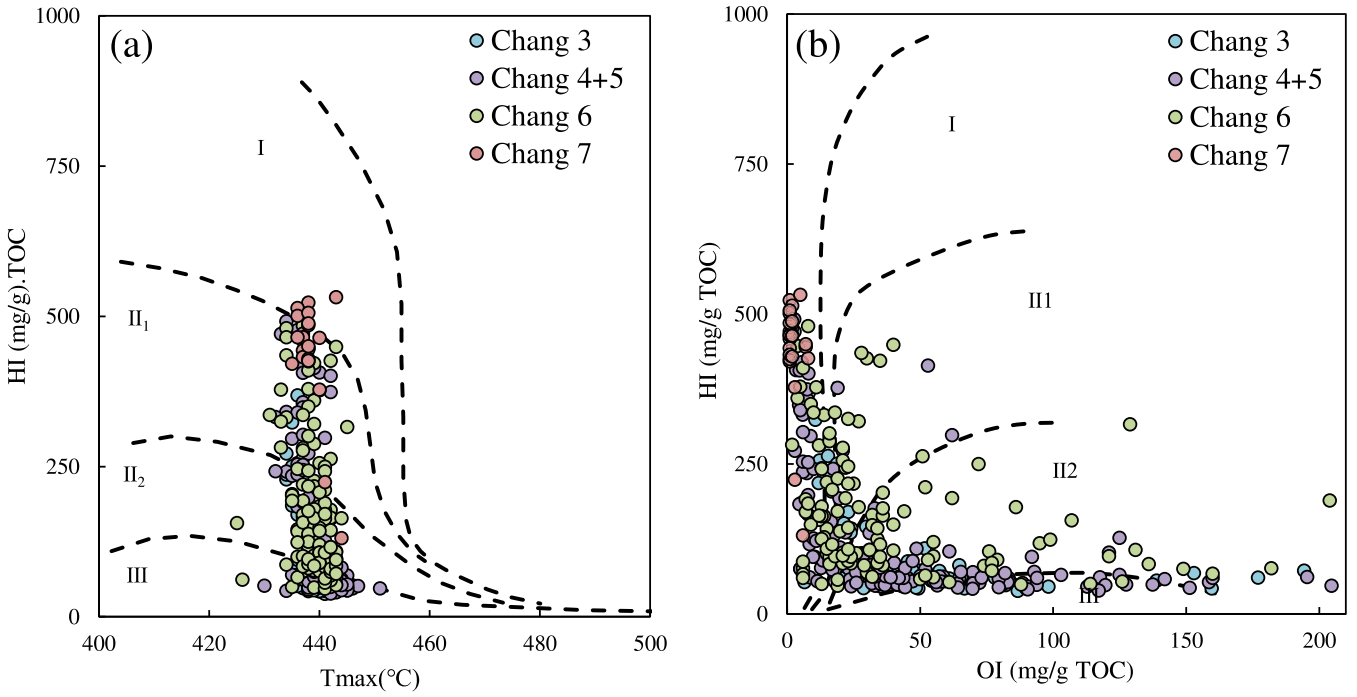

Figure 2. Cross-plots of T_{max} vs HI (a) and OI vs HI (b) showing the classification of organic matter types in the Yanchang source rocks from Chang 3 to Chang 8 members.

2. GEOLOGICAL SETTING

The Ordos Basin is a Mesozoic basin, developed in the Middle Triassic, Middle to Late Triassic, and Early to Middle Jurassic, with abundant terrestrial input and gradual expansion of the lake surface. Regional uplift occurred during deposition, resulting in intermittent deposition, so the Yanchang Formation suffered from different degrees of erosion. The Ordos Basin can be divided into five tectonic units: the Tianhuan sag, the western edge fold-thrust belt, the Weibei uplift, the Yimeng uplift, and the Jinxi fold belt (Figure 1). The study object, well Z101, is located in the Weibei uplift. The Weibei uplift is 200 km long from east to west and 50 km wide from north to south. The Caledonian tectonic movement led to the Permian angular unconformity and strong deformation. The thrust fault was obvious during the Yanshan movement, and the basinal pulling-apart fault subsided during the Himalayan period. The deposition of the Yanchang Formation was accompanied by a complete development of the palaeolake basin, which expanded, then shrank, and then expanded again until its extinction. The stratigraphy is more than 900 m thick, and the objective bed of the study is more than 300 m thick, involving the source rocks of the Chang 3, Chang 4, Chang 5, Chang 6, Chang 7, and Chang 8 members.

3. MATERIALS AND METHODS

This work carried out a high-resolution and systematic core sampling of well Z101 in the YQ city, southern Ordos Basin, and the well location is shown in Figure 1. The lithology of the samples is gray and black, black mud shale, black oil sandstone, gray and dark gray mud siltstone, and gray and dark gray silt mudstone (Figure 1). The samples range from Chang 3 to 8 members of the Yanchang Formation. Representative samples were selected for organic and inorganic geochemical analyses. The tests included total organic matter content, organic carbon and kerogen stable carbon isotopes, aliphatic and aromatic hydrocarbons, gas chromatography−mass spectrometry, stable carbon isotopic compositions of individual hydrocarbons, and major/trace elements.

3.1. Total Organic Carbon and Rock Pyrolysis. Well-ground samples (500 mg) were immersed in 10% HCl and heated in a water bath at 50 °C for 36 h to remove the carbonates and dolomites (inorganic carbon). Dried samples were mixed well and then 5−10 mg was analyzed, and the reaction gas products (CO_2) were carried by helium flow to a copper reactor where excess O_2 was consumed to produce CuO. The products were carried through a packed GC column that provided separation of the combustion gases, which were detected by a thermal conductivity detector. The evolved carbon fraction was measured and converted to TOC and recorded as the mass weight percentage of the rock.

Rock pyrolysis of samples was performed on a Rock-Eval instrument. Well-ground samples (30−50 mg) were weighed and then transferred to a crucible for pyrolysis in the Rock-Eval. The measured parameters include the free hydrocarbon content (S_1 mg/g), source potential (S_2 mg/g), hydrogen and oxygen index (HI and OI mg/g), and thermal maturity (T_{max} °C).

3.2. Bulk Stable Carbon Isotopic Compositions. The carbon isotope determination of organic matter and kerogen was performed by high-temperature combustion. Well-ground samples (500 mg) were immersed in 10% HCl and heated in a water bath at 50 °C for 36 h to remove the carbonates and dolomites (inorganic carbon). The dried samples were set in a vacuum quartz tube with high-purity oxygen. The organic material was converted into CO_2 by combustion at 850 °C for 15 min. CO_2 was separated and purified by different refrigerants, liquid nitrogen and dry ice, and was collected in a gas collection bottle. The reproducibility was within 0.3‰, and the isotopic compositions of all samples are reported relative to the international Vienna Peedee Belemnite (VPDB) standard.

3.3. Crushing, Solvent Extraction, and Fractionation. The bulk shales were crushed into powder in a rotary mill. The

https://doi.org/10.1021/acsomega.2c07382
ACS Omega 2023, 8, 5820−5835

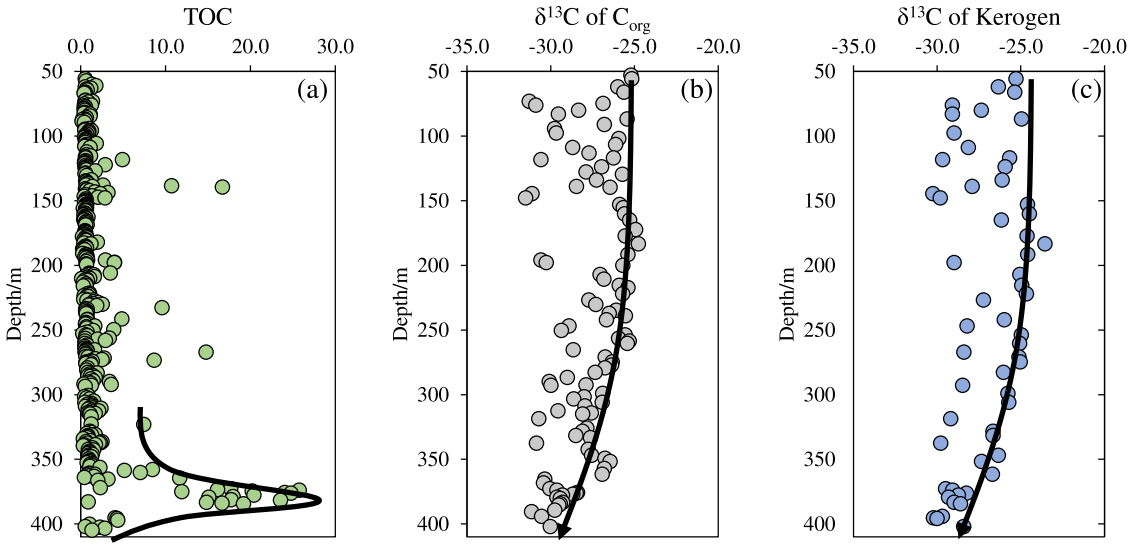

Figure 3. Variation of (a) TOC; (b) δ^{13}C values of organic matter; and (c) δ^{13}C values of kerogen with burial depth for the samples from the Yanchang source rocks.

homogenized powdered samples were extracted using a Soxhlet apparatus with a mixture of dichloromethane-methanol (9:1 v/v) for 72 h. Then, the extracts were fractionated using two-phase silica gel column liquid chromatography. Total hydrocarbons were separated from polar compounds by eluting the extractable organic matter (EOM) with *n*-hexane/dichloromethane (4:1 v/v). Then, the total hydrocarbons were separated into aliphatic hydrocarbons, which were collected by eluting with *n*-hexane, and aromatic hydrocarbons, which were collected by eluting with *n*-hexane/dichloromethane (4:1 v/v).

3.4. Gas Chromatography−Mass Spectrometry (GC−MS). Gas chromatography−mass spectrometry (GC−MS) analyses of the aliphatic and aromatic hydrocarbon fractions were performed on an Agilent GC (6890N) coupled to an Agilent Mass Selective Detector (5975B) equipped with a J&W DB-5MS fused silica column (length 60 m, inner diameter 0.25 mm, film thickness 0.25 μm). The inlet was held at 35 °C for 3 min and then was programmed to 310 °C (0.4 min. isothermal) at a rate of 700 °C/min. Samples were injected in a splitless mode. The temperature of the GC oven was initially held at 35 °C for 4 min and was programmed to 310 °C at 4 °C/min and then was held for 40 min. Helium (99.999%) was used as the carrier gas. The carrier gas flow rate (constant flow) was 1.5 mL/min. The ion source of the mass spectrometer was operated in the electron ionization (EI) mode at 70 eV. The MS data were acquired in full scan mode. The relative abundance of compounds was determined from peak areas (using selected mass chromatograms for the integration of the compounds).

3.5. Gas Chromatography−Isotope Ratio−Mass Spectrometry (GC−IR−MS). An aliquot of the saturated fraction from selected samples was separated into purified n-alkanes and branched/cyclic alkanes by urea adduction. An Agilent 6890 gas chromatograph (GC, 30 m, inner diameter 0.25 mm, film thickness 0.25 μm; constant flow 1.0 mL/min) coupled to a Thermo MAT 253 through a GC-C-III combustion (with NiO/CuO/Pt at 950 °C) interface was used to determine the ^{13}C of the selected compounds. The samples were injected at 290 °C using the splitless mode (60 s). The GC oven temperature was initially held at 50 °C for 2 min and was programmed to increase to 120 °C at 25 °C/min and then to 310 °C at 5 °C/min, where it was maintained isothermally for 8 min. Helium was used as the carrier gas. A standard mixture of *n*-alkanes with known δ^{13}C values was analyzed to test the accuracy of the instrument. The isotopic compositions of all samples are reported relative to the international Vienna Peedee Belemnite (VPDB) standard and were determined at least twice. The standard deviations of the replicates were calculated to estimate reproducibility. The reproducibility was within 0.4‰.

4. RESULTS AND INTERPRETATIONS

4.1. Bulk Geochemistry. The organic matter types of the main five source rock members of the Yanchang Formation are classified in Figure 2a. The organic matter types of source rocks in the Yanchang Formation are mainly III−II_2−II_1 type. The Chang 7 member has mainly II_1 type organic matter, and individual samples have I type organic matter; the Chang 6 member has mainly III type−II_2 type organic matter, and II_1 type organic matter is partially distributed; the Chang 3, Chang 4 + 5, and Chang 8 members have wider distributions of II_1 type−II_2 type−III type organic matter.

Based on the cross-plot of the OI-HI index for organic matter type identification, as shown in Figure 2b, the source rocks of the Chang 7 section have the highest HI and lower OI index, with the HI index range 480−500 mg/g and the OI index range 0−20 mg/g. The source rocks of the Yanchang Formation mainly consist of I type organic matter, with partial II_1-II_2 type organic matter. The Chang 7 member source rocks have the better organic matter type. An initial assessment based on the OI−HI index identification indicates that the organic matter source is dominated by aquatic algae and aquatic microorganisms, with less contribution from terrestrial organic matter.

In Figure 3, there are four rises of TOC (up to 25.8%) in the Yanchang Formation, and the HI also increases in response, which may indicate increasingly better preservation conditions for organic matter. The stable carbon isotopic compositions of organic matter and kerogen have similar decreasing trends (approx. −25 to −32‰ for organic matter; approx. −24 to −31‰ for kerogen, respectively) to the Chang 3 to the Chang 8 members. The Chang 7 member source rocks are more depleted in ^{13}C than other members. This suggests that the organic carbons in different members have different primary producers or different ecological preservation conditions.

https://doi.org/10.1021/acsomega.2c07382
ACS Omega 2023, 8, 5820−5835

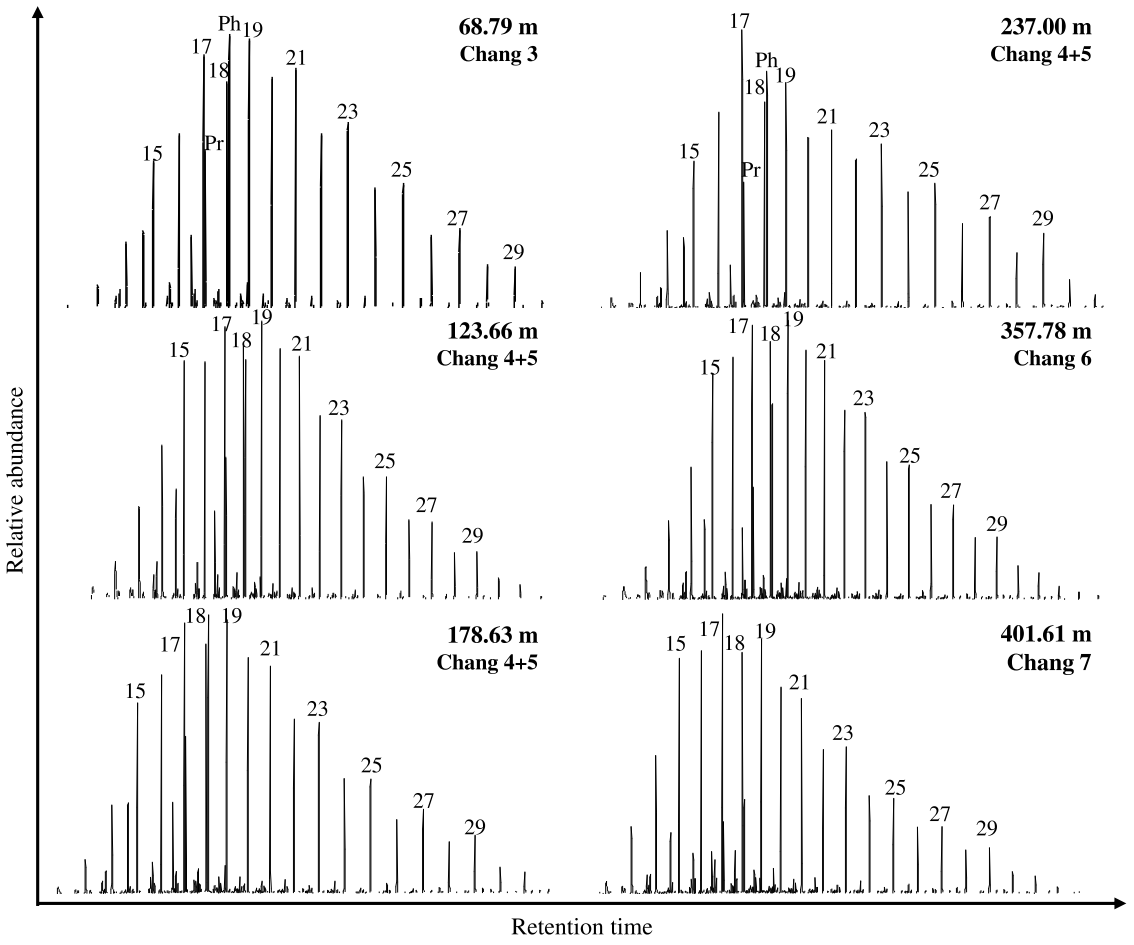

Figure 4. Representative mass chromatograms of m/z 57 showing the distribution of *n*-alkanes of the Yanchang source rock samples in the Ordos Basin. Numbers on peaks are *n*-alkane carbon numbers; Pr = phytane and Ph = phytane.

4.2. Molecular Geochemistry. *4.2.1. n-Alkanes and Isoprenoids.* The aliphatic fractions of the Yanchang samples have abundant *n*-alkanes ranging from $C_{13}-C_{32}$, with a maximum at *n*-C_{17} or *n*-C_{18} (Figure 4 and Table 1). All samples contain the highest relative abundance of short-to-long-chain *n*-alkanes ($<C_{21}$). There is a prominent odd-over-even carbon number preference for the middle-to-long-chain *n*-alkanes (CPI = 1.01−1.21). The average $\sum 20-/\sum 21+$ *n*-alkane ratio is 3.4. There are no obvious differences between the samples across from the Chang 3 to Chang 8 member samples, which suggests that the organic matter inputs are stable during the deposition. This also suggests more contribution from aquatic organisms than from terrigenous higher plants to the organic matter in the Yanchang Formation source rocks.

The pristane/phytane ratio (Pr/Ph) is less than 1.0 for almost all of the samples, with a few exceptions (Table 1). The Pr/Ph of the Chang 7 member samples ranges from 0.49 to 0.64. The cross-plots of the Ph/*n*-C_{18} and Pr/*n*-C_{17} ratios range from 0.26 to 3.05 and 0.31 to 1.64, respectively, which indicates that the *n*-alkanes, pristane, and phytane are generally derived from type II organic matter that was deposited in an anoxic bottom water environment (Figure 5). An increasing trend of thermal maturity based on the Ph/*n*-C_{18} and Pr/*n*-C_{17} ratios was observed from the Chang 3 to Chang 8 member samples.

4.2.2. Hopanes and Steranes. On the m/z 191 mass chromatograms, C_{30} 17α,21β(*H*) hopane is predominant, followed in abundance by C_{29} norhopane (Figure 6). Most of the samples have C_{29} hopane $<C_{30}$ hopane ratios. C_{19-26} triterpanes, Ts (18α-22,29,30-trisnorneohopane), Tm (17α-22,29,30-trisnorhopane), and homohopanes ($C_{31}-C_{33}$) are present in very low concentrations. Gammacerane is also present in low concentrations (gammacerane index GI: 0.01−0.13), and there is no C_{35} homohopane predominance over C_{34} homohopane. Oleanane and tricyclic and tetracyclic diterpanes are absent. The C_{21} tricyclic terpane has a comparable abundance to the C_{23} tricyclic terpane for almost all of the samples, and C_{19} and C_{20} tricyclic terpanes are present in low relative abundances. The Ts/(Ts + Tm) ratios range from 0.02 to 0.7, indicating a relatively low thermal maturity for the Yanchang Formation source rocks. Trace absence of oleanane and of diterpanes[12] in all slices are suggestive of limited angiosperm and vascular plant contributions to organic matter (OM).[13] Similarly low abundances of C_{19} and C_{20} tricyclic terpanes are consistent with the low input of terrigenous OM.[14]

On the m/z 217 mass chromatograms, the regular steranes have both C_{27} predominance over C_{28} and C_{29} and C_{29} predominance over C_{28} and C_{27} for all samples, suggesting a varying aquatic organism input to the steranes (C_{27}/C_{29} ranges from 0.53 to1.91). Consistent with the relative distribution of terpanes, the C_{27}/C_{29} $\alpha\alpha\alpha$ R sterane ratio may thus indicate the relative contribution of different algae rather than being a terrigenous vs aqueous organic input proxy. C_{30} dinosteranes (m/z 98 and m/z 231) are absent in all samples. However, the C_{29} regular steranes/C_{29} $\alpha\beta$ hopane ratios (St/H) are less than

https://doi.org/10.1021/acsomega.2c07382
ACS Omega 2023, 8, 5820−5835

Table 1. Organic Geochemical Parameters of the Chang Member Source Rocks in the Yanchang Formation, Ordos Basin[a]

depth/m	∑C21−/∑C22+	Pr/Ph	Pr/n-C_{17}	Ph/n-C_{18}	GI	Ts/(Ts + Tm)	St/H
10	1.56	0.54	0.99	2.05	0.04	0.34	0.21
33	2.21	0.53	0.69	1.46	0.07	0.39	0.58
69	1.32	1.41	1.39	1.28	0.07	0.08	0.46
83	1.15	0.52	0.89	1.51	0.06	0.19	0.07
85	1.73	0.41	1.21	3.05	0.05	0.48	0.22
89	2.11	1.00	0.79	1.23	0.05	0.02	0.12
95	0.89	0.43	1.09	2.61	0.08	0.07	0.41
97	1.96	0.37	0.75	2.46	0.06	0.52	0.14
105	1.27	0.83	0.96	1.55	0.01	0.03	0.48
109	1.73	0.47	0.79	1.83	0.09	0.49	0.52
116	1.34	0.42	0.93	2.28	0.09	0.50	0.23
122	1.49	0.53	0.79	1.56	0.10	0.58	0.24
124	1.15	0.53	0.99	2.09	0.04	0.36	0.15
130	1.29	0.81	1.17	2.00	0.06	0.11	0.88
134	1.03	0.56	1.03	2.02	0.09	0.53	0.30
138	2.17	0.49	0.69	1.67	0.05	0.48	0.24
148	1.20	0.43	0.80	1.91	0.05	0.42	0.34
153	1.21	0.48	0.73	2.02	0.05	0.26	0.18
155	0.92	0.52	1.00	2.10	0.13	0.32	0.27
163	1.02	0.55	0.96	2.31	0.11	0.12	0.73
166	0.98	0.77	1.01	1.73	0.05	0.11	0.41
168	1.45	0.86	1.20	1.80	0.08	0.09	0.13
172	0.54	1.08	1.42	1.09	0.09	0.29	0.46
177	1.34	0.61	0.70	1.22	0.03	0.20	0.15
179	1.24	0.55	0.86	2.25	0.09	0.09	1.01
183	0.97	1.64	1.23	1.22	0.06	0.06	0.43
188	1.00	0.52	1.04	2.29	0.10	0.29	0.31
192	1.27	0.54	0.80	2.03	0.13	0.19	0.35
198	1.51	0.51	0.64	1.44	0.06	0.57	0.17
210	1.34	0.48	0.68	1.57	0.07	0.57	0.21
223	1.72	0.71	0.87	1.30	0.07	0.27	0.23
232	2.37	0.52	0.52	1.12	0.06	0.38	0.49
237	1.68	0.51	0.55	1.20	0.05	0.53	0.27
246	1.61	0.46	0.67	1.56	0.05	0.41	0.51
250	1.87	0.43	0.67	1.86	0.03	0.38	0.48
254	2.92	1.66	0.98	0.97	0.08	0.08	0.45
267	2.87	0.58	0.41	0.87	0.06	0.37	0.61
272		0.55	0.75	1.43	0.10	0.60	0.43
290	2.45	0.41	0.39	1.07	0.03	0.33	0.43
305	1.52	0.41	0.47	1.24	0.04	0.37	0.40
311	1.78	0.39	0.43	1.26	0.03	0.38	0.33
329	1.08	0.58	0.62	1.14	0.03	0.51	0.42
339	1.34	0.48	0.40	0.85	0.03	0.41	0.40
348	2.16	0.72	0.36	0.60	0.02	0.59	0.25
358	1.76	0.55	0.41	0.84	0.03	0.44	0.32
366	1.16	0.64	0.43	0.66	0.04	0.61	0.19
373	3.37	0.51	0.32	0.74	0.03	0.15	0.37
378	2.63	0.56	0.31	0.63	0.03	0.15	0.24
382	2.12	0.55	0.32	0.66	0.02	0.16	0.24
384	2.43	0.62	0.32	0.58	0.02	0.16	0.26
387	1.46	0.58	0.36	0.63	0.02	0.15	0.24
389	0.99	0.62	0.56	0.79	0.03	0.16	0.25
395	9.57	0.49	0.08	0.23	0.03	0.38	

[a]Pr = pristane; Ph = phytane; GI = gammacerane/C_{30} $\alpha\beta$ hopane; St/H = C_{29} ($\alpha\alpha\alpha$ + $\alpha\beta\beta$) steranes/C_{29} $\alpha\beta$ hopanes (based on areas in m/z 191 and m/z 217); Ts = 18α(H)-22,29,30-trisnorneohopane; Tm = C_{27} 17α(H)-22,29,30-trisnorhopane.

1.0 for all samples analyzed (0.34 on average), with a slight decrease from the Chang 3 to Chang 8 member samples. The Chang 7 samples have the lowest St/H average value (0.26). This may suggest that the primary produced organic matter has been reworked by the heterotrophic bacteria with a likely minor contribution from photosynthetic bacteria.

4.3. Carbon Isotopic Composition of *n*-Alkanes and Isoprenoids. The $\delta^{13}C$ values of the individual n-alkanes of the

https://doi.org/10.1021/acsomega.2c07382
ACS Omega 2023, 8, 5820−5835

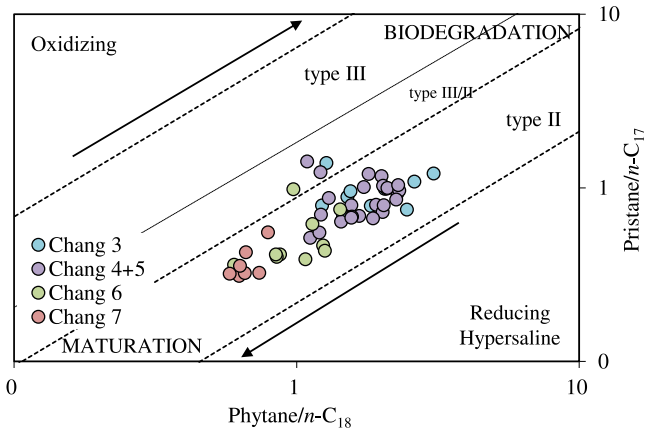

Figure 5. Cross-plot of Ph/n-C_{18} and Pr/n-C_{17} ratios of the Yanchang source rock samples in the Ordos Basin.

representative Yanchang source rocks are shown (Figure 7a and Table 2). The $\delta^{13}C$ values of all samples range from −30.6 to −39.8‰ (with two anomaly data points). The shapes of their n-alkane isotope profiles are identical in the range of n-C_{14} to n-C_{19} alkanes and have negative slopes to different extents and an abrupt positive shift from the n-C_{22} to n-C_{25} alkanes. The average $\delta^{13}C$ values of the n-C_{14} to n-C_{20} n-alkanes range from −31.2 to −34.3‰, and the average $\delta^{13}C$ values of the n-C_{20} to n-C_{30} n-alkanes range from −33.1 to −37.4‰. The low molecular weight (LMW) n-alkanes are 2.8‰ enriched in ^{13}C relative to the HMW n-alkanes, therefore suggesting mixed organic matter sources. The depletion of ^{13}C in the HMW n-alkanes supports a non-terrigenous origin of these alkanes,[15−17] as n-alkanes from higher plants are usually enriched in ^{13}C relative to those from aquatic organisms.[18,19] This negative shift in the HMW n-alkanes may suggest an enhanced aquatic-sourced organic input.[20]

In comparison, the n-alkane isotope profiles of the Chang 7 member source rocks (Figure 7b) differ from the profiles of other member source rocks (Figure 7c). They are relatively more flat and less negatively shifted at the range of n-C_{20} to n-C_{27} alkanes, suggesting a more uniform and stable organic carbon source, which has been attributed to a dominantly phytoplanktonic or heterotrophic bacterial source.[20] The Chang 7 samples have isotopically heavier mid-chain n-alkanes (n-C_{20} to n-C_{27}) than the rest samples.

The $\delta^{13}C$ values of pristane range from −31.0 to −34.5‰ and of phytane range from −31.6 to −35.4‰. Pristane is enriched in ^{13}C by a ∼1.0‰ relative to that of phytane. Pristane and phytane both have increasing $\delta^{13}C$ values with increasing burial depths. The $\delta^{13}C$ values of n-alkanes slightly increase with increasing burial depths. However, there is no correlation between the $\delta^{13}C$ values of the n-alkanes, pristane, and phytane with the thermal maturity parameters, and the Yanchang samples have a relatively low thermal maturity in the early−middle oil window.

5. DISCUSSION

5.1. General Evaluation of Organic Matter in the Yanchang Formation. The pyrolysis result (Tmax, HI, and OI) suggests that the Yanchang Formation source rocks contain all types of organic matter. The Chang 7 member source rocks have higher quality and TOC than other member source rocks.

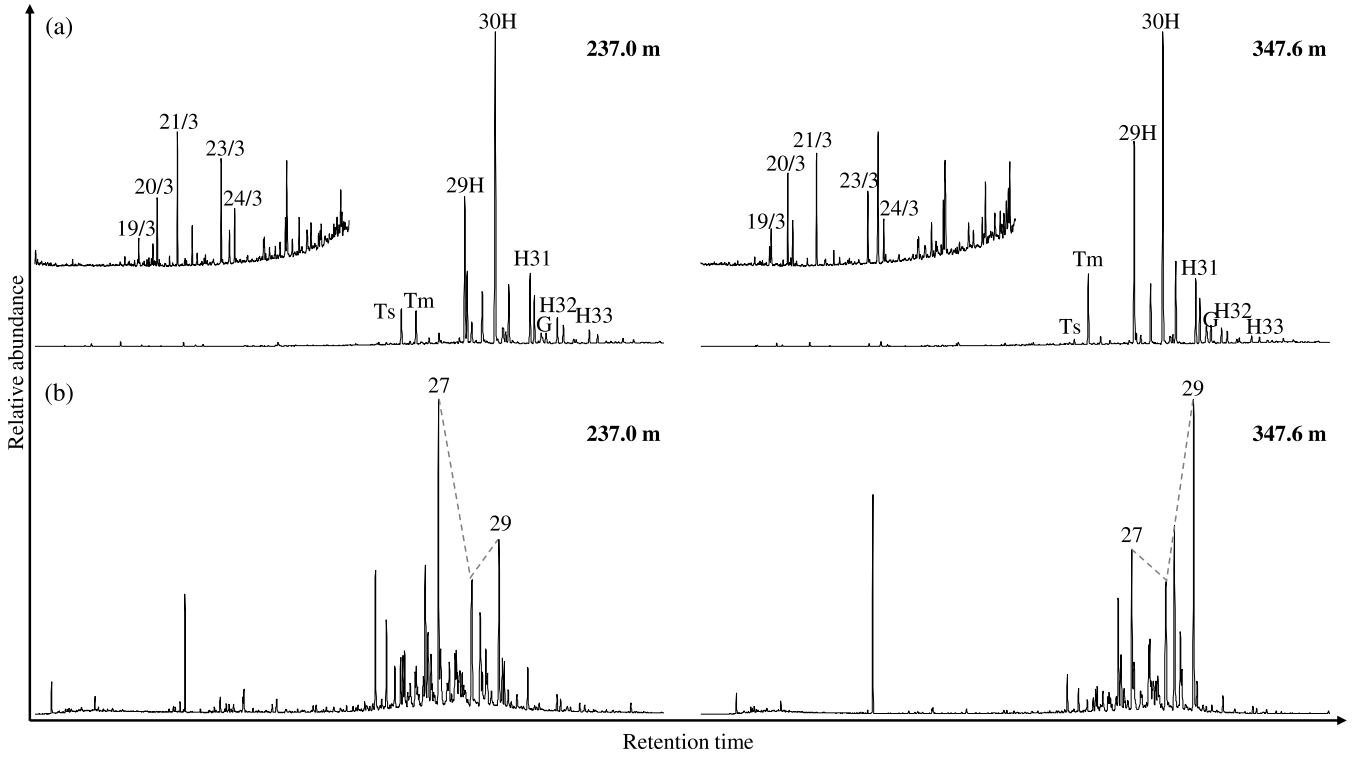

Figure 6. Representative mass chromatograms of m/z 191 (a) showing the distribution of terpanes in the Yanchang source rock samples in the Ordos Basin. Representative partial m/z 217 mass chromatograms (b) showing the distribution of regular steranes in the Yanchang source rock samples in the Ordos Basin. Two insets are the expanded parts of the m/z 191 traces. Peak assignments: 19/3 to 29/3 = C_{19}−C_{29} tricyclic terpanes, 24/4 = C_{24} tetracyclic terpane, Ts = 18α(H),22,29,30-trisnorneohopane, Tm = 17α(H),22,29,30-trisnorhopane, 30H = C_{30} $\alpha\beta$ hopane, 29H = C_{29} $\alpha\beta$ hopane, G = gammacerane, and H31 to H35 = C_{31}−C_{35} $\alpha\beta$ homohopanes (S + R). Numbers on peaks are sterane ($\alpha\alpha\alpha$R isomer) carbon numbers.

https://doi.org/10.1021/acsomega.2c07382
ACS Omega 2023, 8, 5820−5835

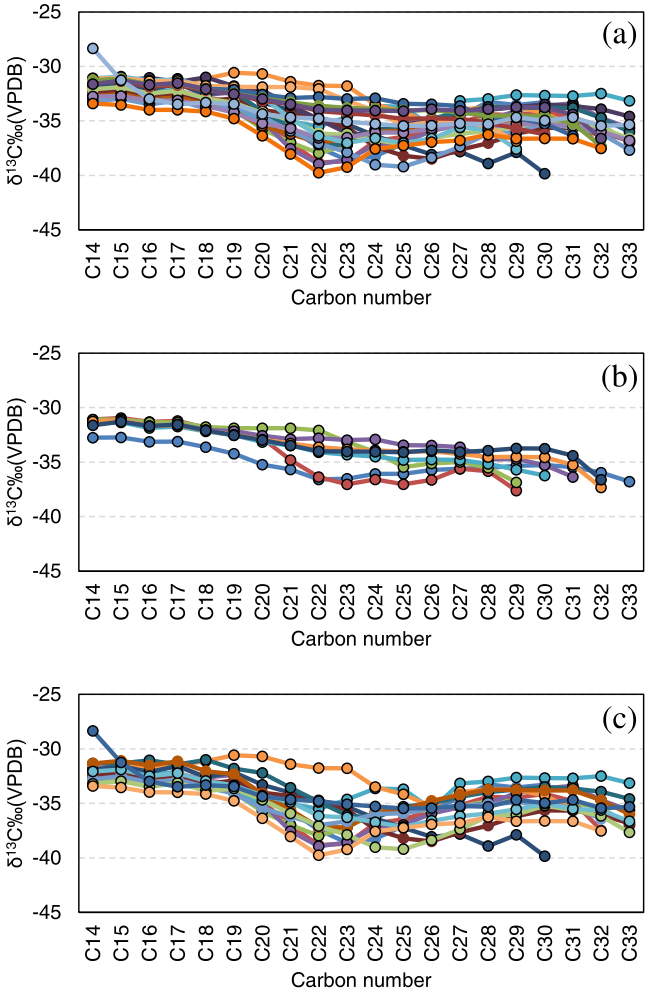

Figure 7. $\delta^{13}C$ values of individual C_{14} to C_{33} *n*-alkanes in the selected Chang member source rocks (a), Chang 7 member source rocks (b), and Chang 3, 4 + 5, 6 member source rocks (c) of the Yanchang Formation, Ordos Basin.

Stable carbon isotopic compositions of organic matter and kerogen (both more depleted in ^{13}C) are consistent with better organic matter preservation for the Chang 7 member source rocks. The LMW *n*-alkanes are typically derived from microbes comprising primary producers and heterotrophs, i.e., algae and bacteria.[21,22] The higher proportions of LMW *n*-alkanes ($\sum 20-/\sum 21+ = 3.4$ on average) for almost all of the Yanchang samples analyzed suggest a higher contribution of aquatic algae and heterotrophic bacteria to the sedimentary OM. This is also reflected by the absence of terrigenous biomarkers (e.g., oleanane or diterpanes). The Ts/(Ts + Tm) ratio (0.33 on average) and the prominent odd-over-even carbon number preference (Figure 4) are indicative of a low level of thermal maturity for the Yanchang OM. An average $\delta^{13}C$ value (−32.6‰) of the *n*-C_{14} to *n*-C_{20} *n*-alkanes suggests that all of the Yanchang OM have a prominent phytoplanktonic origin.[10,23,24] The difference in *n*-alkane isotope profiles (at the range of the *n*-C_{20} to *n*-C_{30} *n*-alkanes) between the Chang 7 member samples and the rest samples (Figure 7b,c) suggests a different ecological and environmental preservation condition for Chang 7 member OM (slightly enriched in ^{13}C). However, the low St/H ratios (0.34 on average, with a general decreasing trend from Chang 3 to Chang 7 members) in the analyzed samples suggest that the samples have a relatively high proportion of bacterial relative to eukaryotic lipid contribution (e.g., see ref 24). This may be partially attributed to the heterotrophic bacterial reworking of primarily produced OM contributing more hopenoid lipids because photosynthetic bacteria (e.g., green sulfur bacteria) contribute only minuscule amounts of OM to bottom sediments.[25] The isoprenoid ratios of Pr/Ph (0.69 on average), Ph/*n*-C_{18}, and Pr/*n*-C_{17} support a generally reducing depositional environment for the Yanchang source rocks. However, very low GI (0.06 on average) discounts the persistent stratification of the water column, and the photic zone euxinia (PZE) was not present as no aryl isoprenoids and C_{40} aromatic carotenoids (e.g., isorenieratane) were observed.[26,27]

5.2. Heterotrophic Bacterial Reworking of Algal-Derived OM. The absence of PZE and water stratification during the deposition of the Yanchang source rocks suggests that there was no obvious chemocline and the water column was not sulfidic, at least not in the photic zone. This is surprising relative to most of the organic-rich shales globally. However, abundant pyrite in the Yanchang source rocks[10,28] suggests that H_2S should be abundant below the photic zone during the deposition. This explains the good correlations of S with various metals such as Fe, U, Cu, Mo, etc. (Figure 8 and Table 3) and their preferential reactions with H_2S forming metal sulfides[29] before feeding green or purple sulfur bacteria in the photic zone. Significant bacterial sulfate reduction (BSR) reduces electron acceptors generating abundant H_2S during early diagenesis.[28] Pristane and phytane have a dominant algal origin and no other sources in this study such as cyanobacteria, phototrophic bacteria, or archaeal membrane lipids.[30] Very low Pr/Ph values (0.69 on average) suggest that the algal-derived phytols suffered less aerobic degradation during settling through thinner oxic water layers, and thus the lower water column or the bottom water were anoxic (not necessarily sulfidic). This anoxic condition can be created by the significant consumption of OM by heterotrophic microbes at the early diagenetic stage.[31−33] This will result in good preservation conditions for Yanchang OM, but the TOC spike in the Chang 7 member remains unclear, and it also remains unclear to what extent the TOC spike is a result of heterotrophic bacterial reworking.

Multiple hypotheses for Yanchang organic-rich shale include high primary productivity,[10,29] magmatic activity,[28,34] marine transgression,[7] etc. Good correlations of TOC with various elements such as Mo, U, Re, Cu, etc. were observed (Figure 9). The detailed mechanism of the fertilization effect by these elements as nutrients have been well discussed,[10,28,35,36] while a proportional adsorption effect has also been noticed during the enrichment of OM,[29,37] and high TOC seems to be a prerequisite condition for metal (e.g., uranium) enrichment in the black shales. One further conflicting view was that U radiation may be toxic to the algae in the oxygenated surface water layers.[38] However, heterotrophic sulfate-reducing bacteria (SRB), for example, *Desulfotomaculum*, have remarkable tolerance and adaptation to high levels of uranium.[39−41] So, various nutrients have positively or negatively impacted the algae or bacteria to different degrees. In short, the prokaryotic heterotrophic bacteria during the deposition of the Chang 7 member have a greater capacity to biosorb radiation (1.9×10^{17} MeV/g rock in the Chang 7 member vs 0.2×10^{17} MeV/g rock in the Chang 3 + 4 + 5 + 6 + 8 members; on average) or the radioactive metals such as U, Mo, and Re than eukaryotic algae (lower St/H ratio, high proportion of bacterial relative to eukaryotic lipids and probably lower $\delta^{13}C$ values of bulk OM or

https://doi.org/10.1021/acsomega.2c07382
ACS Omega 2023, 8, 5820−5835

Table 2. Compound Specific Stable Carbon Isotope Data for *n*-Alkanes in the Selected Chang Member Source Rocks of the Yanchang Formation, Ordos Basin

depth/m	C14	C15	C16	C17	C18	C19	C20	C21	C22	C23	C24	C25	C26	C27	C28	C29	C30	C31	C32	C33
223	−32.7	−32.5	−32.8	−32.7	−33.1	−33.2	−34.7	−35.7	−37.4	−38.6	−38.3	−37.1	−35.4	−34.6	−33.3	−33.5	−33.3			
232	−32.6	−32.3	−32.7	−32.2	−32.9	−33.2	−34.8	−37.0	−38.8	−38.7	−36.8	−36.5	−35.6	−35.2	−34.4	−34.5	−34.1	−34.8	−37.5	
237	−32.8	−32.6	−33.0	−32.5	−33.6	−34.0	−35.7	−37.0	−38.0	−37.2	−35.9	−35.8	−35.6	−35.3	−34.8	−34.8	−34.9	−34.9	−35.4	−37.0
246	−31.9	−31.5	−32.0	−31.6	−32.6	−32.4	−35.0	−37.6	−38.9	−38.6	−37.2	−37.0	−35.9	−35.3	−35.0	−34.1	−33.6	−33.4	−34.7	−35.7
250	−32.1	−31.7	−32.4	−32.1	−33.4	−34.0	−35.0	−35.0	−35.5	−34.6	−33.6	−33.7	−35.5	−33.2	−33.0	−32.6	−32.7	−32.7	−32.5	−33.2
254		−31.2	−31.9	−31.5	−31.1	−30.6	−30.7	−31.4	−31.8	−31.8	−33.5	−34.2	−35.3	−34.0	−33.7	−33.7	−34.3	−35.5		
267	−31.9	−31.6	−32.1	−31.6	−32.6	−32.1	−33.3	−34.0	−34.7	−35.3	−36.4	−37.2	−38.1	−37.8	−38.9	−37.9	−39.9			
272	−32.3	−32.2	−32.7	−32.5	−33.2	−32.9	−34.0	−34.3	−34.9	−35.6	−37.4	−38.2	−38.5	−37.6	−37.0	−36.2	−35.6	−35.7	−36.0	−36.8
290	−32.3	−32.0	−32.3	−31.9	−33.1	−33.9	−35.7	−37.0	−38.0	−38.0	−36.6	−36.3	−35.6	−34.9	−33.8	−34.8	−33.6	−44.4	−33.7	−47.0
305	−31.4	−31.3	−31.1	−31.0	−31.8	−31.8	−32.2	−33.6	−34.9	−36.1	−36.3	−35.3	−35.0	−34.4	−34.0	−33.7	−33.5	−33.6	−33.9	−34.6
311	−31.4	−31.1	−31.5	−31.1	−32.0	−32.3	−34.1	−35.6	−37.2	−37.2	−35.8	−35.6	−34.8	−34.2	−33.7	−33.8	−33.8	−33.8	−34.7	−36.0
329	−32.8	−32.5	−33.1	−32.8	−33.5	−34.1	−35.5	−36.2	−37.0	−36.6	−36.0	−35.9	−35.5	−35.2	−35.1	−34.9	−35.1	−35.4	−36.4	
339	−33.2	−33.0	−33.5	−33.1	−33.9	−33.6	−34.7	−35.9	−37.1	−37.9	−39.0	−39.2	−38.4	−37.4	−36.2	−36.0	−35.2	−35.6	−36.2	−37.7
348	−32.8	−32.7	−33.0	−32.7	−33.6	−33.5	−34.1	−34.3	−35.0	−36.4	−37.6	−37.7	−37.3	−37.1	−37.0	−37.0	−37.8	−39.6	−47.8	
358	−32.1	−31.9	−32.5	−32.2	−32.9	−33.4	−34.3	−34.9	−36.1	−36.3	−36.7	−37.2	−36.6	−36.2	−35.9	−35.6	−35.0	−35.5	−35.6	−36.6
366	−32.8	−32.7	−33.1	−33.1	−33.6	−34.2	−35.2	−35.7	−36.6	−36.5	−36.1	−36.1	−35.7	−35.6	−35.5	−35.3	−35.3	−35.5	−36.0	−36.8
373	−31.1	−30.9	−31.3	−31.2	−31.9	−32.1	−32.8	−34.8	−36.4	−37.0	−36.6	−37.0	−36.6	−35.6	−35.8	−37.6				
378	−31.1	−31.1	−31.4	−31.3	−31.8	−31.9	−31.9	−31.9	−32.1	−33.1	−34.1	−35.5	−35.1	−35.0	−35.5	−36.9				
382	−31.3	−31.2	−31.7	−31.6	−32.0	−32.2	−32.6	−32.9	−32.8	−33.0	−32.9	−33.4	−33.5	−33.6	−34.8	−34.7	−35.3	−36.4		
384	−31.4	−31.4	−31.9	−31.7	−32.2	−32.5	−33.2	−33.5	−34.1	−34.3	−34.5	−34.8	−34.8	−34.8	−35.2	−35.7	−36.2			
387	−31.3	−31.1	−31.7	−31.6	−32.1	−32.5	−32.9	−33.3	−33.6	−33.8	−33.9	−34.0	−34.0	−34.2	−34.5	−34.5	−34.6	−35.2	−37.3	
389	−31.6	−31.3	−31.7	−31.5	−32.1	−32.5	−33.0	−33.5	−34.0	−34.0	−34.1	−34.1	−33.9	−34.1	−33.9	−33.7	−33.8	−34.4	−36.6	

https://doi.org/10.1021/acsomega.2c07382
ACS Omega 2023, 8, 5820−5835

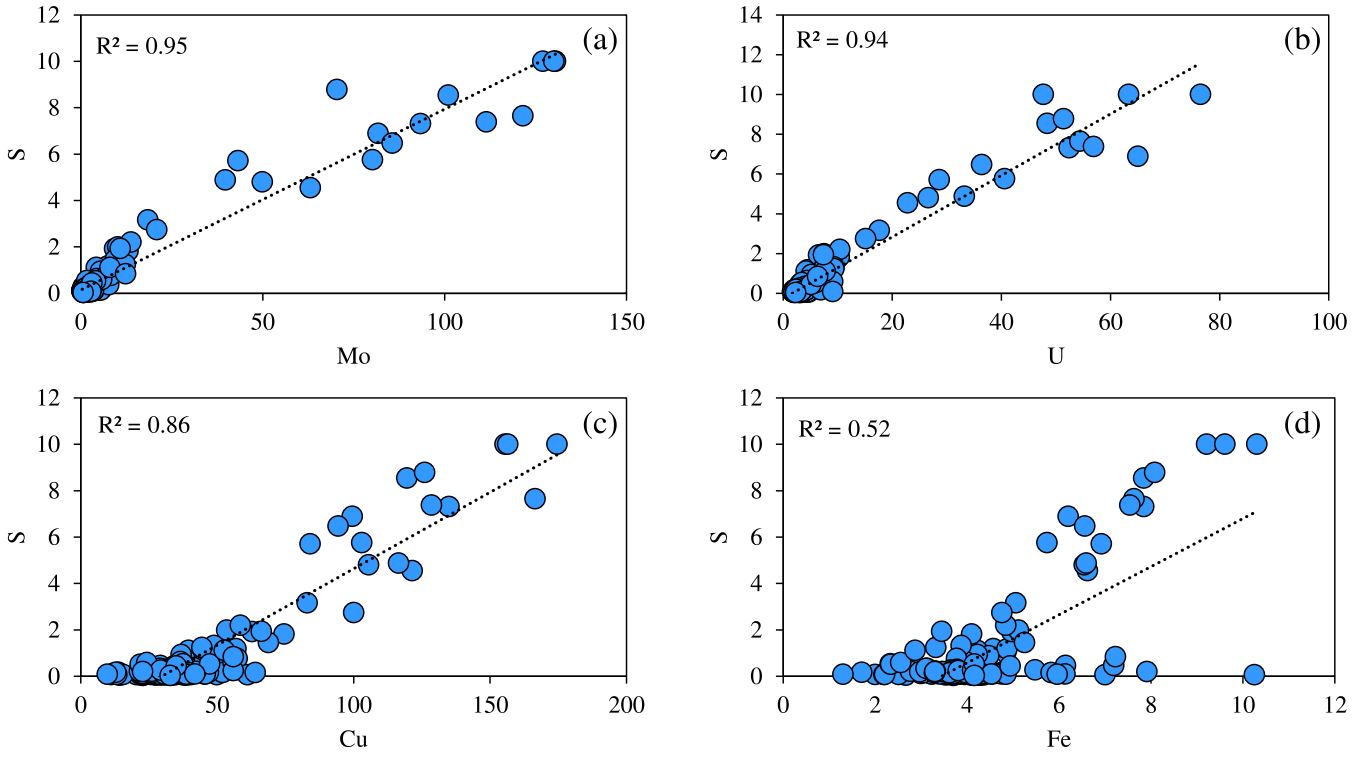

Figure 8. Cross-plots of S with Mo (a), U (b), Cu (c), and Fe (d) in the Yanchang source rocks. Elements (ppm).

kerogen). Overall, the molecular and isotopic data suggest that the SRB play an important role in organic carbon cycling/export and may be responsible for the much better OM preservation in the Chang 7 member.

5.3. Shift in the Mode of Microbial Respiration Recorded by a Comparison of the ^{13}C of Short-Chain *n*-Alkanes and Isoprenoids. Due to the relatively uniform algal origin of the primary photosynthates, *n*-alkanes, pristane, and phytane can be used to distinguish the exact organic source contribution in the Yanchang Formation. The C_{14-18} *n*-alkanes are typically derived from microbes comprising primary producers and heterotrophs, i.e., algae and bacteria, whereas pristane and phytane are typically derived from phytol side chains of the chlorophylls a and b (cyanobacteria and/or algae).[30] Theoretically, the relatively enriched ^{13}C values (−32.6‰) for the C_{14-20} *n*-alkanes are suggestive of mixed contributions from bacteria or algae.[18] The weighted average $\delta^{13}C$ values of C_{17+18} *n*-alkanes and pristane + phytane can represent different carbon cycling/export pathways and can provide a way of distinguishing various source contributions.[42,43]

Variations in the $\delta^{13}C$ of multisource-derived acyclic isoprenoids pristane, phytane, and short-chain *n*-alkanes (*n*-C_{17} and *n*-C_{18}) were observed in the studied samples (Table 4). The *n*-C_{17} and *n*-C_{18} alkanes are isotopically lighter than pristane and phytane if derived from primary producers (such as algae and cyanobacteria) through the mevalonate pathway, whereas they are isotopically heavier if derived from heterotrophs utilizing primary photosynthates or bacterial biomass.[42,43] The weighted average $\delta^{13}C$ values of C_{17+18} *n*-alkanes range from −30.8 to −35.3‰, and the weighted average $\delta^{13}C$ values of pristane + phytane range from −31.6 to −35.0‰. Pristane and phytane in the Chang 3 and 4 + 5 members are mostly ^{13}C enriched relative to *n*-C_{17} and *n*-C_{18} (Figure 10), which indicates that the *n*-C_{17} and *n*-C_{18} alkanes were derived mainly from lipids of primary producers, e.g., algae. Pristane and phytane in the Chang 6 and 7 members are mostly ^{13}C depleted relative to *n*-C_{17} and *n*-C_{18}, which indicates that the *n*-C_{17} and *n*-C_{18} alkanes were derived mainly from lipids of various heterotrophic bacteria. The $\Delta\delta$ values (where $\Delta\delta$ = [average $\delta^{13}C$ of *n*-C_{17} + *n*-C_{18}] − [average $\delta^{13}C$ of Pr + Ph]) increase progressively from Chang 3 (−1.39−0.65; −0.51 on average) through Chang 4 + 5 (−1.77−1.47; −0.19 on average) and Chang 6 (−0.88−0.87; 0.15 on average) to Chang 7 (0.12−1.18; 0.95 on average) members (Table 4). A positive $\Delta\delta$ value indicates heterotrophic origins, and a negative $\Delta\delta$ value indicates autotrophic origins (Figure 10a).

A clear increasing trend was observed from Chang 3 to 7 members, which strongly supports that there was a major change in the carbon cycling/export mode during the deposition of the Chang member OM. The isotopic enrichment of *n*-C_{17} + *n*-C_{18} *n*-alkyl carbon chains results from the heterotrophic processing of primary photosynthate or dominant inputs of isotopically heavy bacterial biomass. This is also supported by the slightly higher average $\delta^{13}C$ values of the *n*-C_{14} to *n*-C_{20} *n*-alkanes in Chang 7 (−32.0‰) than in the Chang 3, 4 + 5, 6, and 8 (−32.8‰) members.

The increasing homohopane index (HHI) with increasing burial depth (Figure 10b) is also consistent with an increasing heterotrophic bacterial activity during early diagenesis, as low HHI values can be used to gauge the extent of redox conditions and bacterial activity.[44−46] A ∼1.0‰ enrichment in ^{13}C of pristane relative to phytane suggests separate origins for the two isoprenoids,[47] additional methanogenic bacteria,[48] or distinct diagenetic pathways,[49] as the phytanyl core of ^{13}C enriched archaeal lipids are one source for phytane that will give rise to relatively positive values of $\delta^{13}C$.[50−52] In short, all of these ^{13}C data suggest that there was a shift in the mode of microbial respiration and carbon cycling from autotrophy in the Chang 3, 4 + 5 members to heterotrophy in the Chang 6 and 7 members.

https://doi.org/10.1021/acsomega.2c07382
ACS Omega 2023, 8, 5820−5835

Table 3. Total Organic Carbon Content and Trace Element Composition of the Selected Chang Member Source Rocks in the Yanchang Formation, Ordos Basin

depth/m	TOC (%)	Cu (ppm)	Fe (ppm)	Mo (ppm)	U (ppm)	S (ppm)
10	2.1	46.2	4.8	6.4	5.4	1.02
11	0.7	30.4	4.8	0.9	3.5	0.21
16	2.5	45.8	4.4	2.9	5.0	0.23
28	0.6	29.4	4.3	0.7	2.9	0.06
30	1.5	25.9	3.1	2.5	3.5	0.34
32	0.5	21.9	7.0	1.0	2.7	0.06
33	1.4	34.9	4.3	3.5	4.7	0.41
34	0.5	27.9	4.1	1.9	3.1	0.05
37	0.6	28.1	4.2	0.4	3.2	0.12
38	0.7	29.0	4.3	0.3	3.0	0.08
38	0.6	28.2	4.4	0.4	2.9	0.11
44	0.6	34.7	4.0	1.6	3.1	0.09
46	0.6	31.5	3.5	1.0	3.0	0.05
55	0.5	25.7	3.8	0.6	2.9	0.07
57	0.6	33.0	4.0	0.5	3.2	0.07
60	1.3	43.2	2.9	3.1	4.9	0.32
61	1.8	50.0	4.3	4.6	4.3	0.52
62	0.5	22.7	3.7	0.7	2.9	0.03
63	1.2	45.2	4.0	3.5	4.0	0.29
63	0.7	37.2	4.3	2.6	4.7	0.06
66	0.5	20.4	10.3	0.5	2.4	0.06
67	0.4	21.7	3.8	0.6	2.6	0.08
73	1.4	51.8	4.4	3.4	4.6	0.57
73	0.9	36.2	4.5	1.6	3.7	0.17
76	1.2	37.4	4.2	1.3	3.8	0.07
77	0.5	26.6	4.3	0.4	3.1	0.12
83	1.1	40.1	4.2	0.9	3.7	0.06
85	0.7	34.2	4.2	2.8	3.6	0.06
87	0.5	27.3	4.1	1.0	3.1	0.05
88	0.1	11.3	2.0	0.5	1.9	0.07
94	1.0	35.8	4.1	1.7	3.3	0.25
95	0.5	29.6	4.2	0.6	2.6	0.11
95	0.5	27.0	4.2	0.6	2.9	0.07
96	1.3	34.2	4.3	2.6	4.0	0.44
97	0.9	38.5	4.2	1.5	3.3	0.04
101	0.4	24.2	3.7	0.9	2.8	0.20
104	0.6	33.7	4.1	0.7	2.7	0.12
106	1.8	49.7	3.7	0.6	3.0	0.16
108	0.5	30.7	4.3	0.6	2.7	0.07
109	1.1	37.5	4.2	2.9	2.9	0.23
115	1.2	40.0	4.1	5.1	4.7	0.14
116	0.5	31.8	4.0	1.4	3.1	0.13
117	0.6	25.2	7.9	0.8	3.0	0.20
118	4.9	56.9	4.1	0.9	4.5	0.28
119	0.6	29.8	4.4	0.5	2.8	0.05
122	2.9	49.8	4.3	0.9	4.5	0.06
124	0.6	31.7	4.4	0.7	3.1	0.17
138	2.6	41.9	4.4	6.6	5.3	0.57
139	16.7	121.5	6.6	63.1	22.8	4.55
144	2.3	56.9	4.6	8.8	6.5	1.19
146	1.3	39.6	4.2	3.9	4.8	0.69
147	2.0	51.6	4.9	7.4	4.5	1.18
148	0.6	33.7	4.1	1.8	2.9	0.07
153	0.6	31.6	4.2	2.2	3.2	0.08
154	0.6	29.2	3.9	0.7	2.7	0.09
155	0.7	34.6	4.1	1.5	3.0	0.06
160	0.6	32.9	4.3	1.0	2.8	0.06
161	0.4	13.7	4.5	0.7	2.0	0.17
162	0.7	32.3	4.2	1.5	3.4	0.15
165	0.4	23.9	3.6	0.7	3.0	0.07
177	0.6	28.7	5.5	0.8	3.0	0.27
183	1.2	45.4	4.6	0.8	3.8	0.10
192	0.7	40.3	4.1	1.3	3.2	0.10
193	0.5	28.3	3.6	3.4	3.2	0.09
196	2.9	46.1	3.9	2.9	4.4	0.34
198	4.0	62.8	5.0	9.3	6.5	1.92
198	4.0	52.0	3.7	1.3	4.2	0.16
199	0.7	33.6	3.7	5.6	2.8	0.14
206	3.5	45.4	3.7	1.3	3.6	0.16
207	1.6	35.1	3.6	1.1	3.7	0.16
209	1.6	39.5	4.2	4.3	4.2	1.11
211	0.7	33.6	3.4	1.7	3.3	0.18
211	0.5	22.0	3.2	0.7	2.6	0.11
212	0.8	34.7	3.8	1.2	3.3	0.14
213	0.3	14.3	2.7	1.1	2.0	0.04
214	0.6	34.1	4.1	1.7	3.1	0.13
215	0.6	32.9	4.4	0.5	2.7	0.11
216	0.3	15.5	2.5	0.7	2.2	0.07
221	1.0	27.5	3.3	1.4	2.9	0.12
223	0.4	11.0	2.2	1.0	1.7	0.07
224	0.9	35.2	3.6	1.3	3.2	0.08
227	1.5	38.4	3.9	2.1	3.4	0.37
228	1.5	38.2	3.9	4.9	4.8	0.72
230	2.5	53.5	5.1	10.2	7.5	1.99
231	1.0	36.3	4.2	2.1	3.7	0.28
231	1.9	47.6	4.5	6.2	6.9	0.88
233	9.6	105.5	6.6	49.9	26.6	4.80
233	0.6	36.4	4.0	0.9	3.0	0.28
235	0.6	34.1	4.0	0.8	3.1	0.13
236	0.6	32.1	4.0	0.5	2.9	0.08
237	0.8	33.6	3.7	3.6	3.3	0.11
241	4.8	55.8	4.0	4.4	6.1	0.59
244	0.6	29.1	6.1	2.3	3.1	0.46
247	1.7	36.8	4.2	5.4	5.2	0.94
247	0.7	30.5	3.7	1.7	3.3	0.10
248	0.7	32.4	4.0	1.4	3.3	0.10
250	3.9	74.5	4.1	13.0	10.3	1.82
250	1.4	41.3	3.8	7.7	5.7	0.37
251	0.7	35.0	4.8	1.9	3.4	0.10
253	0.2	13.2	2.2	0.9	2.0	0.07
254	0.6	37.3	4.9	0.8	3.7	0.08
256	3.4	46.8	3.4	2.4	3.4	0.16
256	0.6	30.0	4.1	0.6	3.1	0.27
260	0.5	23.5	4.3	0.5	2.7	0.09
263	0.5	25.6	4.3	0.4	2.8	0.10
264	0.5	27.3	3.8	0.5	2.8	0.12
265	0.7	27.5	3.3	0.9	3.0	0.21
266	0.7	32.7	3.5	3.5	3.9	0.13
268	0.6	29.1	3.9	0.4	3.0	0.14
269	0.6	26.6	3.6	0.4	2.7	0.14
271	0.8	28.1	3.2	0.9	2.8	0.10
272	1.7	45.6	3.4	1.7	3.6	0.09
273	8.6	84.0	6.9	43.2	28.6	5.71
274	1.4	36.5	4.0	4.3	4.4	0.63
275	0.6	22.6	3.0	0.7	2.5	0.12
276	0.6	32.4	3.9	0.8	3.3	0.26
281	0.7	26.2	3.1	0.8	2.7	0.15
283	0.8	36.1	3.9	2.9	4.3	0.22

https://doi.org/10.1021/acsomega.2c07382
ACS Omega 2023, 8, 5820−5835

Table 3. continued

depth/m	TOC (%)	Cu (ppm)	Fe (ppm)	Mo (ppm)	U (ppm)	S (ppm)
283	1.9	38.4	7.2	2.3	3.7	0.46
285	0.9	37.2	4.0	2.0	3.6	0.14
288	1.1	32.7	3.6	2.1	3.6	0.23
290	3.4	58.5	4.8	13.8	10.4	2.20
291	1.1	26.1	2.8	3.0	3.9	0.21
292	3.6	48.8	3.9	10.7	9.3	1.32
293	1.3	57.3	3.8	8.2	6.9	0.77
301	0.9	61.1	4.1	1.8	3.7	0.06
303	1.1	31.1	3.8	2.9	4.6	0.29
305	1.5	31.4	3.7	2.2	3.7	0.26
306	0.5	21.5	3.7	2.5	2.9	0.21
308	1.3	42.1	3.7	1.7	3.9	0.21
309	1.2	38.7	3.5	2.1	3.7	0.20
310	1.2	38.9	3.6	1.0	3.7	0.15
311	0.9	37.4	2.3	1.7	3.4	0.54
312	2.1	68.8	5.3	9.5	7.7	1.45
315	1.1	63.9	4.0	2.4	3.6	0.16
317	1.2	34.0	3.0	3.0	4.0	0.19
328	1.1	32.3	5.8	1.4	4.2	0.16
329	1.2	55.9	3.8	2.5	3.8	0.24
331	1.3	28.9	3.1	2.4	4.0	0.34
332	0.8	30.6	6.1	2.0	2.8	0.10
337	2.3	44.4	3.3	12.3	9.3	1.24
339	1.7	21.8	2.3	4.6	8.3	0.52
339	0.4	12.8	1.7	1.6	6.9	0.17
341	1.4	24.2	2.6	5.8	9.1	0.59
344	1.0	36.6	4.3	1.3	3.2	0.17
345	0.9	36.8	3.3	1.2	3.3	0.21
348	0.9	29.3	4.1	3.1	3.0	0.26
348	1.3	47.2	4.2	4.1	5.9	0.53
351	1.1	39.6	3.3	1.0	3.3	0.15
353	0.8	38.7	6.0	1.2	3.0	0.08
354	1.1	22.7	3.3	1.2	2.4	0.20
358	8.4	116.5	6.6	39.7	33.2	4.88
360	7.0	83.0	5.1	18.4	17.6	3.16
362	0.8	41.8	4.5	1.0	3.3	0.09
363	1.6	35.0	4.9	3.1	5.1	0.44
364	0.4	9.7	1.3	2.8	9.1	0.08
365	11.7	135.0	7.8	93.4	52.4	7.31
365	3.2	100.0	4.8	20.9	15.1	2.74
372	2.3	52.6	2.9	8.0	7.7	1.11
374	25.8	155.5	10.3	127.0	76.5	10.00
376	24.0	99.5	6.2	81.7	65.0	6.89
376	24.8	119.5	7.8	101.0	48.4	8.54
378	20.4	156.5	9.2	130.5	63.3	10.00
379	17.9	174.5	9.6	130.0	47.7	10.00
379	15.1	126.0	8.1	70.4	51.4	8.78
381	17.7	103.0	5.7	80.2	40.6	5.76
382	23.5	166.5	7.6	121.5	54.4	7.65
384		94.3	6.6	85.6	36.4	6.47
384	19.2	128.5	7.5	111.5	56.9	7.38
395	4.0	66.2	3.5	10.9	7.4	1.93
396	4.3	55.9	7.2	12.3	6.3	0.84

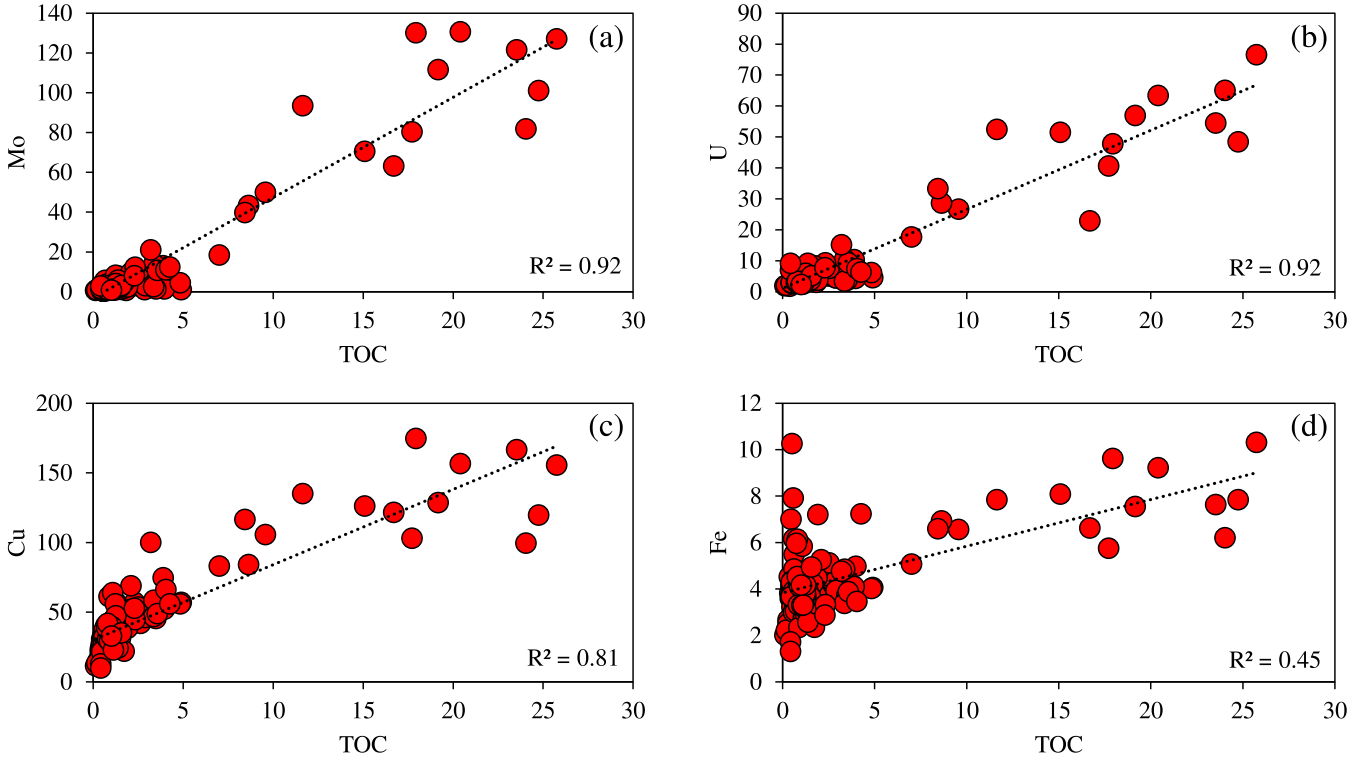

Figure 9. Cross-plots of TOC with Mo (a), U (b), Cu (c), and Fe (d) in the Yanchang source rocks. TOC (%), elements (ppm).

The elevated heterotrophic processing of primary photosynthates or dominant inputs of isotopically heavy bacterial biomass during the deposition of the Chang 7 member has greatly improved OM preservation. In addition to the good correlations of TOC with Fe, U, Cu, Mo, etc. at the Chang 7 member (e.g., Figure 9), most of the biomarker proxies show no

https://doi.org/10.1021/acsomega.2c07382
ACS Omega 2023, 8, 5820−5835

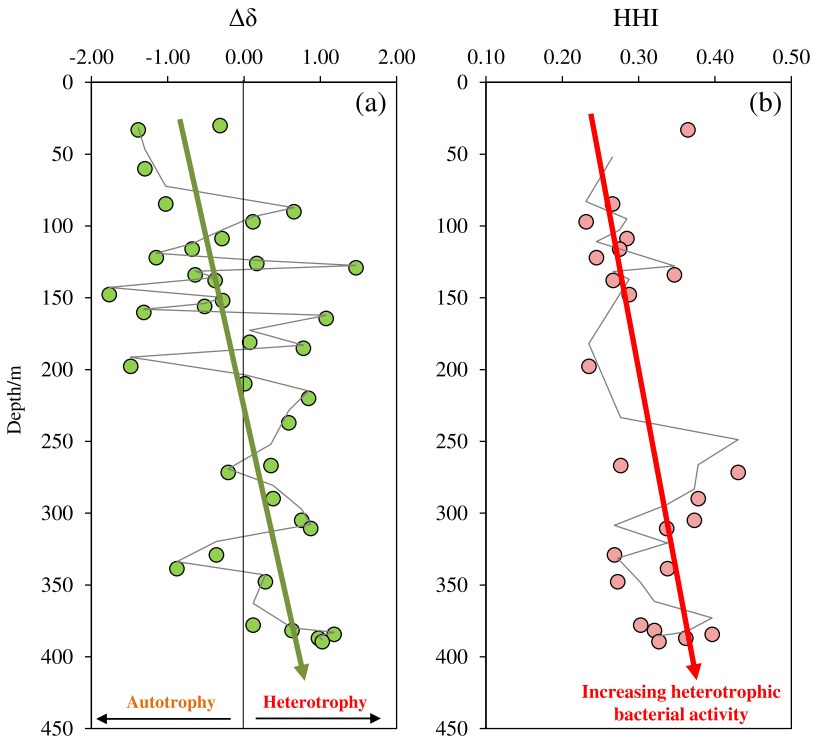

Figure 10. Variation of $\Delta\delta$ = [average δ^{13}C of n-C_{17} + n-C_{18}] − [average δ^{13}C of Pr + Ph] (a) and HHI = homohopane index (b) vs stratigraphic depth.

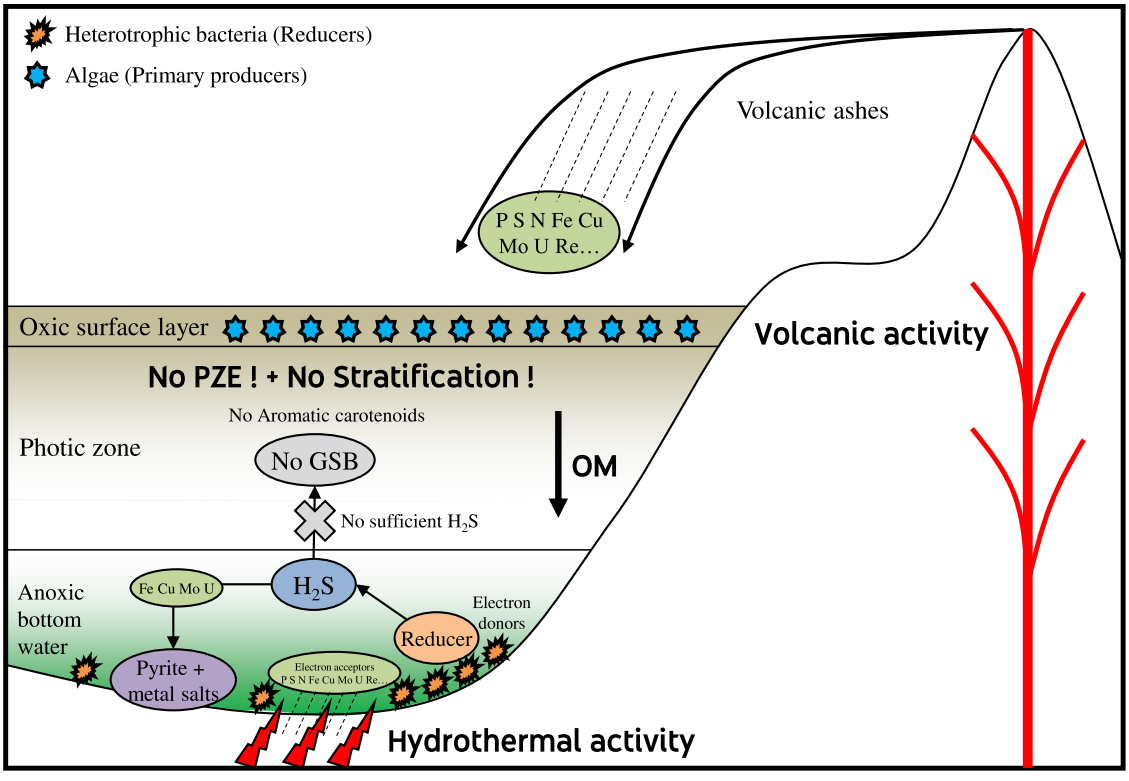

Figure 11. Schematic illustration of the carbon cycling in the Yanchang source rocks. OM = organic matter, GSB = green sulfur bacteria, and PZE = photic zone euxinia.

significant mathematical correlations with the TOC or $\Delta\delta$ values, suggesting the independent ^{13}C assessment of the microbial respiration and carbon cycling.[43] A weak positive correlation (r = 0.45) of the $\Delta\delta$ values with the V/(V + Ni) ratio may indicate the association between bacterial reworking and reducing water conditions.

This shift of carbon cycling may be largely attributed to the external ecological and environmental forcings on the microbes in the water column, including climate change, magmatic

https://doi.org/10.1021/acsomega.2c07382
ACS Omega 2023, 8, 5820−5835

Table 4. Homohopane Index and Compound Specific Stable Carbon Isotope Data for *n*-Alkanes, Pristane, and Phytane in the Selected Chang member Source Rocks of the Yanchang Formation, Ordos Basin[a]

depth/m	HHI	Δδ	*n*-C_{17}	*n*-C_{18}	Pr	Ph
30		−0.31	−33.33	−33.91	−32.71	−33.91
33	0.36	−1.39	−34.15	−34.87	−33.04	−33.20
60		−1.30	−35.04	−35.48	−33.60	−34.33
85	0.27	−1.03	−34.76	−35.40	−33.82	−34.28
90		0.65	−33.59	−33.45	−33.04	−35.32
97	0.23	0.12	−34.39	−35.35	−34.54	−35.43
109	0.28	−0.29	−33.71	−34.54	−33.36	−34.31
116	0.28	−0.68	−33.80	−34.86	−33.48	−33.81
122	0.24	−1.15	−34.74	−35.50	−33.75	−34.19
126		0.17	−33.93	−34.20	−33.48	−34.99
129		1.47	−32.31	−32.00	−32.00	−35.25
134	0.35	−0.64	−33.17	−34.41	−32.93	−33.37
138	0.27	−0.38	−32.66	−33.83	−32.59	−33.15
148	0.29	−1.77	−34.75	−35.73	−33.17	−33.78
153		−0.28	−33.30	−34.07	−32.67	−34.14
155		−0.52	−34.20	−34.76	−33.29	−34.64
160		−1.31	−34.20	−34.76	−32.20	−34.13
163		1.08	−32.08	−32.12	−32.02	−34.33
181		0.07	−33.15	−32.95	−31.91	−34.34
185		0.78	−30.99	−30.60	−31.03	−32.12
198	0.23	−1.49	−33.61	−34.96	−32.42	−33.18
210		0.01	−32.99	−33.89	−33.19	−33.71
220		0.84	−32.73	−33.07	−32.81	−34.68
237		0.59	−32.52	−33.57	−33.37	−33.89
267	0.28	0.35	−31.57	−32.60	−32.23	−32.64
272	0.43	−0.21	−32.48	−33.20	−32.17	−33.10
290	0.38	0.38	−31.92	−33.15	−32.77	−33.06
305	0.37	0.76	−31.00	−31.81	−31.65	−32.67
311	0.34	0.87	−31.14	−32.05	−32.37	−32.57
329	0.27	−0.36	−32.81	−33.50	−32.21	−33.38
339	0.34	−0.88	−33.13	−33.86	−32.22	−33.01
348	0.27	0.28	−32.66	−33.57	−32.67	−34.12
378	0.30	0.12	−31.35	−31.78	−31.73	−31.64
382	0.32	0.63	−31.56	−32.05	−32.11	−32.75
384	0.40	1.18	−31.72	−32.18	−32.89	−33.37
387	0.36	0.98	−31.59	−32.11	−32.91	−32.74
389	0.33	1.03	−31.55	−32.10	−32.79	−32.91

[a]HHI = $C_{35}/(C_{35} + C_{34})$ homohopanes; Δδ = [average $\delta^{13}C$ of *n*-C_{17} + *n*-C_{18}] − [average $\delta^{13}C$ of Pr + Ph]; Pr = pristane; Ph = phytane.

activity, marine transgression, etc. The Chang 7 samples have the lowest average St/H value (0.26) than the Chang 3, 4 + 5, 6 samples (0.32, 0.37, and 0.40, respectively). A stronger bacterial lipid contribution to the OM and stronger heterotrophic origins were confirmed in the Chang 7 member. Considering the absence of water stratification and PZE, abrupt geological events of hydrothermal or volcanic activities[6,34,53] are likely to bring abundant nutrients (electron acceptors) and induce the extensive bacterial reworking (reducers as electron donors) of primarily-produced algal OM. The anoxia at the bottom-water interface was further enhanced and a much better OM preservation condition was formed (Figure 11).

6. CONCLUSIONS

This work presents a combined molecular and carbon isotopic compositional assessment of a range of high prokaryotic-lipid-contributed source rocks in the Yanchang Formation, Ordos Basin. The Chang 7 member has higher quality source rocks than other Chang members. The low maturity biomarker features suggest that there were no water stratification, PZE, and no obvious change in the OM source, and the water column is generally anoxic. A comparison of the $\delta^{13}C$ of Pr and Ph with the $\delta^{13}C$ of the *n*-C17 and *n*-C18 alkanes provides an approach to clarify the source contributions and carbon cycling mode. These results reveal a shift in the mode of microbial respiration and carbon cycling from autotrophy to heterotrophy across the Chang 3, 4 + 5, 6 members to the Chang 7 member and provide evidence for the elevated extent of anaerobic heterotrophic bacterial reworking and organic carbon mineralization at the Chang 7 member. Although the possible external forcings on this shift in the mode of carbon cycling are inconclusive, this finding improves our understanding of heterotrophic bacterial activity control on the OM preservation and biological shift and may be a significant supplement for understanding the ecological or environmental forcings in the Yanchang Formation, Ordos Basin.

AUTHOR INFORMATION

Corresponding Authors

Huiyuan Xu − *State Key Laboratory of Shale Oil and Gas Enrichment Mechanisms and Effective Development, Beijing 100083, China; School of Energy Resources, China University of Geosciences (Beijing), Beijing 100083, China; Petroleum Exploration and Production Research Institute, SINOPEC, Beijing 100083, China;* orcid.org/0000-0003-3124-4254; Phone: +86 (0) 10-56608086; Email: xuhuiyuan.syky@sinope.com, huiyuan.xu@hdr.mq.edu.au, xuhuiyuan.ian@hotmail.com

Quanyou Liu − *State Key Laboratory of Shale Oil and Gas Enrichment Mechanisms and Effective Development, Beijing 100083, China; Institute of Energy, School of Earth and Space Sciences, Peking University, Beijing 100871, China;* Email: liuqy.syky@sinope.com

Zhiquan Li − *School of Environmental Science and Engineering, Sun Yat-Sen University, Guangzhou 510006, China;* Email: lizhiquan@163.com

Dujie Hou − *School of Energy Resources, China University of Geosciences (Beijing), Beijing 100083, China;* Email: hdj@cugb.edu.cn

Xu Han − *School of Energy Resources, China University of Geosciences (Beijing), Beijing 100083, China;* Email: hanxuboy@126.com

Authors

Peng Li − *State Key Laboratory of Shale Oil and Gas Enrichment Mechanisms and Effective Development, Beijing 100083, China; Petroleum Exploration and Production Research Institute, SINOPEC, Beijing 100083, China*

Pengpeng Li − *Institute of Energy, School of Earth and Space Sciences, Peking University, Beijing 100871, China*

Biqing Zhu − *Institute of Energy, School of Earth and Space Sciences, Peking University, Beijing 100871, China*

Complete contact information is available at: https://pubs.acs.org/10.1021/acsomega.2c07382

Notes

The authors declare no competing financial interest.

https://doi.org/10.1021/acsomega.2c07382
ACS Omega 2023, 8, 5820−5835

■ ACKNOWLEDGMENTS

This research was supported by the National Natural Science Foundation of China (Grant Nos. 42141021, U20B6001 & 42102185).

■ REFERENCES

(1) Schidlowski, M. A 3,800-million-year isotopic record of life from carbon in sedimentary rocks. *Nature* **1988**, *333*, 313−318.
(2) Sorokin, Y. I. Role of carbon dioxide and acetate in biosynthesis by sulphate-reducing bacteria. *Nature* **1966**, *210*, 551−552.
(3) Demaison, G. J.; Moore, G. T. Anoxic environments and oil source bed genesis. *Org. Geochem.* **1980**, *2*, 9−31.
(4) Pedersen, T. F.; Calvert, S. E. Anoxia vs productivity: what controls the formation of organic-carbon-rich sediments and sedimentary rocks? *AAPG Bull.* **1990**, *74*, 454−466.
(5) Tyson, R. V.; Pearson, T. H. Modem and ancient continental shelf anoxia: an overview. *Geol. Soc., London, Spec. Publ.* **1991**, *58*, 1−24.
(6) Liu, Q.; Zhu, D.; Jin, Z.; Meng, Q.; Li, S. Influence of volcanic activities on redox chemistry changes linked to the enhancement of the ancient Sinian source rocks in the Yangtze craton. *Precambrian Res.* **2019**, *327*, 1−13.
(7) Jin, X.; Baranyi, V.; Caggiati, M.; Franceschi, M.; Wall, C. J.; Liu, G.; Schmitz, M. D.; Gianolla, P.; Ogg, J. G.; Lu, G.; et al. Middle Triassic lake deepening in the Ordos Basin of North China linked with global sea-level rise. *Global Planet. Change* **2021**, *207*, No. 103670.
(8) Xu, Z.; Liu, L.; Liu, B.; Wang, T.; Zhang, Z.; Wu, K.; Feng, C.; Dou, W.; Wang, Y.; Shu, Y. Geochemical characteristics of the Triassic Chang 7 lacustrine source rocks, Ordos Basin, China: Implications for paleoenvironment, petroleum potential and tight oil occurrence. *J. Asian Earth Sci.* **2019**, *178*, 112−138.
(9) Duan, Y. Geochemical characteristics of crude oil in fluvial deposits from Maling oilfield of Ordos Basin, China. *Org. Geochem.* **2012**, *52*, 35−43.
(10) Zhang, W.; Yang, W.; Xie, L. Controls on organic matter accumulation in the Triassic Chang 7 lacustrine shale of the Ordos Basin, central China. *Int. J. Coal Geol.* **2017**, *183*, 38−51.
(11) Burdige, D. Preservation of Organic Matter in Marine Sediments: Controls, Mechanisms, and an Imbalance in Sediment Organic Carbon Budgets? *Chem. Rev.* **2007**, *107*, 467−485.
(12) Otto, A.; Wilde, V. Sesqui-, di-, and triterpenoids as chemosystematic markers in extant conifers-a review. *Bot. Rev.* **2001**, *67*, 141−238.
(13) Simoneit, B. R. T.; Grimalt, J. O.; Wang, T. G.; Cox, R. E.; Hatcher, P. G.; Nissenbaum, A. Cyclic terpenoids of contemporary resinous plant detritus and of fossil woods, ambers and coals. *Org. Geochem.* **1986**, *10*, 877−889.
(14) Noble, R. A.; Alexander, R.; Kagi, R. I.; Nox, J. K. Identification of some diterpenoid hydrocarbons in petroleum. *Org. Geochem.* **1986**, *10*, 825−829.
(15) Metzger, P.; Largeau, C.; Casadevall, E. Lipids and Macromolecular Lipids of the Hydrocarbon-Rich Microalga *Botryococcus braunii*. Chemical Structure and Biosynthesis. Geochemical and Biotechnological Importance. In *Progress in the Chemistry of Organic Natural Products*; Herz, W.; Kirby, G. W.; Steglich, W.; Tamm, C., Eds.; Springer, 1991; pp 1−70.
(16) Lichtfouse, É.; Derenne, S.; Mariotti, A.; Largeau, C. Possible algal origin of long chain odd *n*-alkanes in immature sediments as revealed by distributions and carbon isotope ratios. *Org. Geochem.* **1994**, *22*, 1023−1027.
(17) Bechtel, A.; Jia, J.; Strobl, S. A. I.; Sachsenhofer, R. F.; Liu, Z.; Gratzer, R.; Püttmann, W. Palaeoenvironmental conditions during deposition of the Upper Cretaceous oil shale sequences in the Songliao Basin (NE China): Implications from geochemical analysis. *Org. Geochem.* **2012**, *46*, 76−95.
(18) Schouten, S.; Breteler, W. C. M. K.; Blokker, P.; Schogt, N.; Rijpstra, W. I. C.; Grice, K.; Baas, M.; Sinninghe Damsté, J. S. Biosynthetic effects on the stable carbon isotopic compositions of algal lipids: Implications for deciphering the carbon isotopic biomarker record. *Geochim. Cosmochim. Acta* **1998**, *62*, 1397−1406.
(19) Chikaraishi, Y.; Naraoka, H.; Poulson, S. R. Hydrogen and carbon isotopic fractionations of lipid biosynthesis among terrestrial (C3, C4 and CAM) and aquatic plants. *Phytochemistry* **2004**, *65*, 1369−1381.
(20) Collister, J. W.; Lichtfouse, E.; Hieshima, G.; Hayes, J. M. Partial resolution of sources of *n*-alkanes in the saline portion of the Parachute Creek Member, Green River Formation (Piceance Creek Basin, Colorado). *Org. Geochem.* **1994**, *21*, 645−659.
(21) Xu, H.; George, S. C.; Hou, D. The occurrence of isorenieratane and 24-*n*-propylcholestanes in Paleogene lacustrine source rocks from the Dongying Depression, Bohai Bay Basin: Implications for bacterial sulfate reduction, photic zone euxinia and seawater incursions. *Org. Geochem.* **2019**, *127*, 59−80.
(22) Xu, H.; Hou, D.; Löhr, S. C.; Liu, Q.; George, S. C. Early diagenetic pyrite cementation influences molecular composition of sedimentary organic matter in the Dongying Depression, China. *Org. Geochem.* **2020**, *144*, No. 104019.
(23) Zhang, W.; Yang, H.; Xia, X.; Xie, G.; Xie, L. Triassic chrysophyte cyst fossils discovered in the Ordos Basin, China. *Geology* **2016**, *44*, 1031−1034.
(24) Brocks, J. J.; Jarrett, A. J. M.; Sirantoine, E.; Hallmann, C.; Hoshino, Y.; Liyanage, T. The rise of algae in Cryogenian oceans and the emergence of animals. *Nature* **2017**, *548*, 578−581.
(25) Manske, A. K.; Glaeser, J.; Kuypers, M. M. M.; Overmann, J. Physiology and Phylogeny of Green Sulfur Bacteria Forming a Monospecific Phototrophic Assemblage at a Depth of 100 Meters in the Black Sea. *Appl. Environ. Microbiol.* **2005**, *71*, 8049−8060.
(26) Koopmans, M. P.; Schouten, S.; Kohnen, M. E. L.; Damsté, J. S. S. Restricted utility of aryl isoprenoids as indicators for photic zone anoxia. *Geochim. Cosmochim. Acta* **1996**, *60*, 4873−4876.
(27) Brocks, J. J.; Schaeffer, P. Okenane, a biomarker for purple sulfur bacteria (*Chromatiaceae*), and other new carotenoid derivatives from the 1640 Ma Barney Creek Formation. *Geochim. Cosmochim. Acta* **2008**, *72*, 1396−1414.
(28) Liu, Q.; Li, P.; Jin, Z.; Liang, X.; Zhu, D.; Wu, X.; Meng, Q.; Liu, J.; Fu, Q.; Zhao, J. Preservation of organic matter in shale linked to bacterial sulfate reduction (BSR) and volcanic activity under marine and lacustrine depositional environments. *Mar. Pet. Geol.* **2021**, *127*, No. 104950.
(29) Yang, H.; Zhang, W.; Wu, K.; Li, S.; Peng, P.; Qin, Y. Uranium enrichment in lacustrine oil source rocks of the Chang 7 member of the Yanchang Formation, Erdos Basin, China. *J. Asian Earth Sci.* **2010**, *39*, 285−293.
(30) Brocks, J. J.; Summons, R. E. Sedimentary Hydrocarbons, Biomarkers for Early Life. In *Treatise on Geochemistry*, 2nd ed.; Turekian, K. K., Ed.; Elsevier, 2014; Vol. *8*, pp 61−103.
(31) Melendez, I.; Grice, K.; Trinajstic, K.; Ladjavardi, M.; Greenwood, P.; Thompson, K. Biomarkers reveal the role of photic zone euxinia in exceptional fossil preservation: An organic geochemical perspective. *Geology* **2013**, *41*, 123−126.
(32) Hebting, Y.; Schaeffer, P.; Behrens, A.; Adam, P.; Schmitt, G.; Schneckenburger, P.; Bernasconi, S. M.; Albrecht, P. Biomarker evidence for a major preservation pathway of sedimentary organic carbon. *Science* **2006**, *312*, 1627−1631.
(33) Killops, S. D.; Killops, V. J. *Introduction to Organic Geochemistry*, 2nd ed.; Blackwell Publishing, 2005.
(34) He, C.; Ji, L.; Wu, Y.; Su, A.; Zhang, M. Characteristics of hydrothermal sedimentation process in the Yanchang Formation, south Ordos Basin, China: Evidence from element geochemistry. *Sediment. Geol.* **2016**, *345*, 33−41.
(35) Langmann, B.; Zakšek, K.; Hort, M.; Duggen, S. Volcanic ash as fertiliser for the surface ocean. *Atmos. Chem. Phys.* **2010**, *10*, 3891−3899.
(36) Duggen, S.; Croot, P.; Schacht, U.; Hoffmann, L. Subduction zone volcanic ash can fertilize the surface ocean and stimulate phytoplankton growth: Evidence from biogeochemical experiments and satellite data. *Geophys. Res. Lett.* **2007**, *34*, No. L01612.

https://doi.org/10.1021/acsomega.2c07382
ACS Omega 2023, 8, 5820−5835

(37) Yang, S.; Schulz, H.-M.; Horsfield, B.; Schovsbo, N. H.; Grice, K.; Zhang, J. Geological alteration of organic macromolecules by irradiation: Implication for organic matter occurrence on Mars. *Geology* **2020**, *48*, 713−717.
(38) Akhtar, K.; Akhtar, M. W.; Khalid, A. M. Removal and recovery of uranium from aqueous solutions by Trichoderma harzianum. *Water Res.* **2007**, *41*, 1366−1378.
(39) Chang, Y.-J.; Peacock, A. D.; Long, P. E.; Stephen, J. R.; McKinley, J. P.; Macnaughton, S. J.; Hussain, A. K. M. A.; Saxton, A. M.; White, D. C. Diversity and Characterization of Sulfate-Reducing Bacteria in Groundwater at a Uranium Mill Tailings Site. *Appl. Environ. Microbiol.* **2001**, *67*, 3149−3160.
(40) Spear, J. R.; Figueroa, L. A.; Honeyman, B. D. Modeling the Removal of Uranium U(VI) from Aqueous Solutions in the Presence of Sulfate Reducing Bacteria. *Environ. Sci. Technol.* **1999**, *33*, 2667−2675.
(41) Benedetto, J. S.; de Almeida, S. K.; Gomes, H. A.; Vazoller, R. F.; Ladeira, A. C. Q. Monitoring of sulfate-reducing bacteria in acid water from uranium mines. *Miner. Eng.* **2005**, *18*, 1341−1343.
(42) Nabbefeld, B.; Grice, K.; Twitchett, R. J.; Summons, R. E.; Hays, L.; Bottcher, M. E.; Asif, M. An integrated biomarker, isotopic and palaeoenvironmental study through the Late Permian event at Lusitaniadalen, Spitsbergen. *Earth Planet. Sci. Lett.* **2010**, *291*, 84−96.
(43) Grice, K.; Cao, C.; Love, G. D.; Bottcher, M. E.; Twitchett, R. J.; Grosjean, E.; Summons, R. E.; Turgeon, S. C.; Dunning, W.; Jin, Y. Photic zone euxinia during the Permian-Triassic superanoxic event. *Science* **2005**, *307*, 707−709.
(44) Schaefer, B.; Grice, K.; Coolen, M. J. L.; Summons, R. E.; Cui, X.; Bauersachs, T.; Schwark, L.; Böttcher, M. E.; Bralower, T. J.; Lyons, S. L.; et al. Microbial life in the nascent Chicxulub crater. *Geology* **2020**, *48*, 328−332.
(45) Roussel, A.; Cui, X.; Summons, R. E. Biomarker stratigraphy in the Athel Trough of the South Oman Salt Basin at the Ediacaran-Cambrian Boundary. *Geobiology* **2020**, *18*, 663−681.
(46) Spaak, G.; Edwards, D. S.; Allen, H. J.; Grotheer, H.; Summons, R. E.; Coolen, M. J. L.; Grice, K. Extent and persistence of photic zone euxinia in Middle−Late Devonian seas − Insights from the Canning Basin and implications for petroleum source rock formation. *Mar. Pet. Geol.* **2018**, *93*, 33−56.
(47) Volkman, J. K.; Zhang, Z.; Xie, X.; Qin, J.; Borjigin, T. Biomarker evidence for *Botryococcus* and a methane cycle in the Eocene Huadian oil shale, NE China. *Org. Geochem.* **2015**, *78*, 121−134.
(48) Brassell, S. C.; Wardroper, A. M. K.; Thomson, I. D.; Maxwell, J. R.; Eglinton, G. Specific acyclic isoprenoids as biological markers of methanogenic bacteria in marine-sediments. *Nature* **1981**, *290*, 693−696.
(49) Schwarzbauer, J.; Littke, R.; Meier, R.; Strauss, H. Stable carbon isotope ratios of aliphatic biomarkers in Late Palaeozoic coals. *Int. J. Coal Geol.* **2013**, *107*, 127−140.
(50) Rowland, S. J.; Robson, J. The widespread occurrence of highly branched acyclic C_{20}, C_{25} and C_{30} hydrocarbons in recent sediments and biota - A review. *Mar. Environ. Res.* **1990**, *30*, 191−216.
(51) Rowland, S. J. Production of acyclic isoprenoid hydrocarbons by laboratory maturation of methanogenic bacteria. *Org. Geochem.* **1990**, *15*, 9−16.
(52) Grice, K.; Schouten, S.; Nissenbaum, A.; Charrach, J.; Damsté, J. S. S. Isotopically heavy carbon in the C_{21} to C_{25} regular isoprenoids in halite-rich deposits from the Sdom Formation, Dead Sea Basin, Israel. *Org. Geochem.* **1998**, *28*, 349−359.
(53) Wenzheng, Z.; Yang, H.; Xie, L.; Yang, Y. Lake-bottom hydrothermal activities and their influence on high-quality source rock development: A case from Chang 7 source rocks in Ordos Basin. *Pet. Explor. Dev.* **2010**, *37*, 424−429.

https://doi.org/10.1021/acsomega.2c07382
ACS Omega 2023, 8, 5820−5835